

Josephson vortex lattice in layered superconductors

Alexei E. Koshelev

Materials Science Division, Argonne National Laboratory, Argonne, Illinois 60439

Matthew J. W. Dodgson

Theory of Condensed Matter Group, Cavendish Laboratory, Cambridge, CB3 0HE, UK

Institut de Physique, Université de Neuchâtel, Rue A. L. Breguet 1, 2000 Neuchâtel, Switzerland and

Department of Physics and Astronomy, University College London, Gower Street, London WC1E 6BT, UK

(Dated: January 13, 2021)

Many superconducting materials are composed of weakly coupled conducting layers. Such a layered structure has a very strong influence on the properties of vortex matter in a magnetic field. This review focuses on the properties of the Josephson vortex lattice generated by the magnetic field applied in the layers direction. The theoretical description is based on the Lawrence-Doniach model in the London limit which takes into account only the phase degree of freedom of the superconducting order parameter. In spite of its simplicity, this model leads to an amazingly rich set of phenomena. We review in details the structure of an isolated vortex line as well as various properties of the vortex lattice, both in dilute and dense limits. In particular, we present an extensive consideration on the influence of the layered structure and thermal fluctuations on the selection of lattice configurations at different magnetic fields.

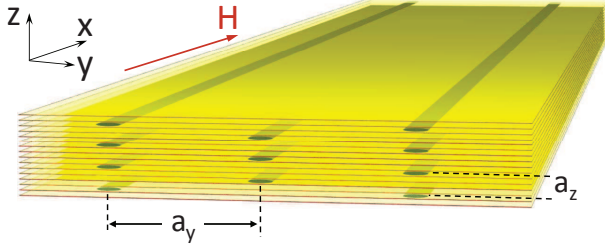


FIG. 1. Illustration of a dilute lattice of Josephson vortices generated in a layered superconductor by magnetic field applied along the layer direction.

I. INTRODUCTION

Layered superconductors are materials made from a stack of alternating thin superconducting layers separated by non-superconducting regions. The superconducting layers are essentially two-dimensional (2D) as long as they are so thin that there is no variation in fields, or in the superconducting order parameter, across each layer. Such structures frequently occur naturally in anisotropic crystals. A layered superconductor can carry supercurrents along the layers, as well as between the layers. This is due to the Josephson tunneling of Cooper pairs¹ across the insulating regions that separate neighboring superconducting layers, i.e., each pair of neighboring layers forms one Josephson junction. In general, the z -axis (Josephson) supercurrents are weaker than the supercurrents along the layers. A mere “layeredness” of atomic structure, however, does not make a material automatically a layered superconductor. When the interlayer electrical coupling is strong enough, this discrete system of layers approximates to a continuous superconductor with uniaxial anisotropy. The case we are interested in here is when the approximation to a

uniaxial continuous superconductor breaks down, which happens when the layer separation d is greater than the z -axis superconducting coherence length, $d \gg \xi_c$.

The most prominent example is the high- T_c cuprate superconductors, discovered in 1986²⁻⁵, which led to a huge interest in physics of layered superconductors. The two most studied cuprate compounds, $\text{YBa}_2\text{Cu}_3\text{O}_7$ (YBCO) and $\text{Bi}_2\text{Sr}_2\text{CaCu}_2\text{O}_x$ (BSCCO), have similar transition temperatures $T_c \approx 90\text{K}$ and represent two important particular cases. YBCO is moderately anisotropic, with the anisotropy factor $\gamma \approx 5 - 7$, and its “layeredness” becomes essential at low temperatures when the c -axis coherence length ξ_c drops below the layer spacing d . On the other hand, BSCCO has a huge anisotropy factor, $\gamma \approx 400 - 1000$, and behaves as a layered superconductor practically in the whole temperature range below T_c . Other naturally layered superconductors include the transition metal dichalcogenides^{6,7} and organic charge-transfer salts formed with the molecule BEDT-TTF^{8,9}. Important new family of atomically layered superconducting materials, iron pnictides and chalcogenides, has been discovered in 2008¹⁰ and are being extensively explored since then, see, e.g., Reviews¹¹⁻¹³. Anisotropy of most compounds is actually not very high and typically they behave as anisotropic three-dimensional materials. There are, however, important exceptions. The most studied compound in which the layered structure is clearly essential is $\text{SmFeAsO}_{1-x}\text{F}_x$ ¹⁴ with T_c up to 55K . For example, Josephson nature of the in-plane vortices at low temperatures has been recently demonstrated in this compound¹⁵. Also, several iron pnictide compounds with extremely high anisotropy have been discovered¹⁶⁻¹⁸. Properties of these compounds remain mostly unexplored due to their rather complicated composition.

All layered superconductors share a very similar general behavior of the vortex matter generated by external

magnetic field, which is insensitive to the microscopic nature of superconductivity inside the layers. Several excellent review articles have been published in the past covering different aspects of the vortex matter in type-II superconductors^{19–23}. Nevertheless, we feel that further progress on the understanding of the Josephson vortices in layered superconductors warrants a specialized review, which will provide much more details and discuss important results obtained in recent years.

This short review narrowly focuses on the vortex lattice which appears at magnetic fields applied along the layers. In this case the flux line winds its phase around an area between two neighboring layers and is called a Josephson vortex in analogy with a vortex in a superconducting tunneling junction. The Josephson vortex contains out-of-plane currents that tunnel via the Josephson effect from layer to layer. The current distribution around vortex is anisotropic. As a consequence, the vortex lattice is also anisotropic, it is a triangular lattice strongly stretched along the layers, see Fig. 1. In addition, the restriction to lie between the layers leads to commensurability effects and an energy barrier to tilting the field away from the layers. There are two very different regimes depending on the strength of the magnetic field B_x . The crossover field scale, B_{cr} , separating these two regimes is set by the anisotropy factor γ and the layer periodicity, d , $B_{cr} = \Phi_0/(2\pi\gamma d^2)$, where $\Phi_0 = hc/2e$ is the flux quantum. In the case of BSCCO this field scale is around 0.5 tesla. In the dilute lattice regime, $B_x < B_{cr}$, the nonlinear cores of Josephson vortices are well separated and the distribution of currents and fields is very similar to that in continuous anisotropic superconductors²⁴. The dense lattice regime is realized at high fields, $B_x > B_{cr}$, where the cores of the Josephson vortices overlap. In this regime the Josephson vortices fill all layers homogeneously²⁵. This state is characterized by rapid oscillations of the Josephson current and by very weak modulation of the in-plane current. In this review we characterize in more detail these two lattice regimes.

Note that we do not consider in this review properties of vortices generated by magnetic field applied perpendicular to the layers, along the c axis.²⁶ The structure of a c -axis vortex is very different from the structure of an in-plane vortex. In layered superconductors the c -axis vortex can be viewed as a stack of weakly coupled point-like pancake vortices. Properties of the pancake vortex lattice were also extensively explored, see, e.g., Reviews 23 and 27 and references therein.

Several experimental techniques have been employed to explore the Josephson vortex lattices. The dilute stretched lattice at small fields ($< 100\text{G}$) has been directly observed in YBCO with Bitter decoration by Dolan *et al.*²⁸, where the elliptical distribution of the flux around each Josephson vortex was also seen. At high fields (> 1 tesla) the commensurability between the c -axis parameter of the Josephson vortex lattice and the interlayer separation leads to magnetic field oscillations which have been observed experimentally in underdoped

YBCO in irreversible magnetization^{29,30} and nonlinear resistivity³¹.

In much more anisotropic BSCCO direct observation of Josephson vortices is not possible. However, when the magnetic field tilted at small angles with respect to the layers, the c -axis field component generates the pancake-vortex stacks which preferably enter the superconductor along the Josephson vortices forming chains. Visualizing the flux of these chains, it is possible to find locations of vertical rows of the Josephson vortices and measure the in-plane lattice parameter a_y . This was done using a variety of visualization techniques, such as Bitter decorations^{32,33}, scanning Hall probes³⁴, Lorentz microscopy^{35,36} and magneto-optical imaging^{37,38}. These observations have been summarized in the Review 39.

Most extensively, properties of the Josephson vortex lattice have been explored in BSCCO using c -axis transport in small-size mesas^{40–44}. These studies revealed a very rich *dynamical* behavior of the lattice, which is beyond the scope of this review. The very important feature is that, due to low dissipation, the Josephson vortex lattice can be accelerated up to very high velocities. It is clear that understanding dynamics is not possible without good understanding of static lattice properties. The dynamic phenomenon closely related to static lattice configurations is magnetic-field oscillations of resistance for very slow lattice motion which have been discovered and explored in small-size BSCCO mesas^{45–49}. The oscillation period may correspond to either flux quantum or half flux quantum per junction depending on the magnetic field and lateral size of the mesa. Interplay between the bulk shearing interaction and the interaction with edges leads to very nontrivial evolution of lattice structures which we consider in this review.

This review is organized as follows. We start in Sec. II in which we present the energy functional and equilibrium equations for the phase and vector potential. In Sec. III we describe the structure and energetics of a single flux line. In Sec. IV we discuss the dilute JVL and consider in details the role of layered structure in selecting lattice configurations. The properties of the dense JVL at high fields are considered in Sec. V. In this regime the structure and energy of the lattice can be evaluated analytically using expansion with respect to the Josephson coupling. In this section we also review the magnetic field dependence of lattice configurations and oscillations of the critical current in finite-size samples. Elastic properties of both dilute and dense lattice are discussed in the corresponding sections. Based on the elastic energies, in Sec. VI we review effects caused by thermal fluctuations.

II. ENERGY FUNCTIONAL AND EQUATIONS FOR THE SUPERCONDUCTING PHASES AND VECTOR-POTENTIAL

Theoretical analysis of the Josephson vortex matter in layered superconductors is based on a phenomenologi-

cal model in which only phase degree of freedom of the superconducting order parameters is taken into account and its amplitude variations are neglected.

$$F_{\text{LLD}}[\phi_n(\mathbf{r}_\parallel), \mathbf{A}(\mathbf{r})] = \int d^3r \frac{B^2}{8\pi} + \sum_n \int d^2r_\parallel \left\{ \frac{E_0}{2} \left(\nabla_\parallel \phi_n + \frac{2\pi}{\Phi_0} \mathbf{A}_{\parallel,n} \right)^2 + \frac{E_J}{d^2} [1 - \cos(\phi_{n+1} - \phi_n + \chi_{n,n+1})] \right\}, \quad (1)$$

where $E_0 = \Phi_0^2 d / (16\pi^3 \lambda_{\text{ab}}^2)$ gives the in-plane phase stiffness and $E_J = E_0 / \gamma^2 = \Phi_0^2 d / (16\pi^3 \lambda_c^2)$ is the phase stiffness for smooth inter-layer phase variations, λ_{ab} and λ_c are the components of the London penetration depth, and $\gamma = \lambda_c / \lambda_{\text{ab}}$ is the anisotropy factor. The z -component of the vector potential enters the tunneling term in the form $\chi_{n,n+1} = (2e/\hbar c) \int_{nd}^{(n+1)d} dz A_z$.⁵⁰ Near the transition temperature the above phase model can be obtained from the celebrated Lawrence-Doniach model⁵¹ by fixing the order-parameter amplitude (London approximation). However, the model is actually more general and describes Josephson properties of layered material in the whole temperature range. Starting from the phase model, a rich variety of the lattice properties can be derived, which we review in this article.

Subject to some given boundary conditions, the configuration of $\{\phi_n, \mathbf{A}\}$ is determined by minimizing the free energy. This leads to a set of differential equations, e.g. minimizing with respect to the phase gives the current-conservation condition,

$$\nabla_\parallel^2 \phi_n + \frac{2\pi}{\Phi_0} \nabla_\parallel \cdot \mathbf{A}_{\parallel,n} = \frac{1}{(\gamma d)^2} (\sin \varphi_{n-1,n} - \sin \varphi_{n,n+1}), \quad (2)$$

with the gauge-invariant phase difference defined as $\varphi_{n,n+1} = \phi_{n+1} - \phi_n + \chi_{n,n+1}$. In this equation the Josephson length, $\Lambda_J = \gamma d$, appears for the first time. This length plays a very important role in layered superconductors, as it determines the scale over which the phase can relax to minimize the Josephson coupling energy without costing too much energy in the gradient term. Three more equations result from minimizing with respect to the three components of the vector potential. We can write these in terms of the electric current density by using the Maxwell equation $\mathbf{j} = (c/4\pi) \nabla \times (\nabla \times \mathbf{A})$, giving,

$$\mathbf{J}_{\parallel,n} = -\frac{2\pi c E_0}{\Phi_0} \left(\nabla_\parallel \phi_n + \frac{2\pi}{\Phi_0} \mathbf{A}_{\parallel,n} \right), \quad (3)$$

$$J_{n,n+1} = -j_J \sin \varphi_{n,n+1}, \quad (4)$$

where $\mathbf{J}_{\parallel,n}$ is the 2D current density in the n th layer and $J_{n,n+1}$ is the current density in the $\hat{\mathbf{z}}$ -direction between the n th and $(n+1)$ th layer which has the maximum value,

$$j_J = \frac{2\pi c E_0}{\Phi_0 (\gamma d)^2}. \quad (5)$$

The four equations (2)–(4), are the starting point for finding the structure of vortices in layered superconductors. In fact, we can make the job of solving this set of equations slightly clearer by combining them to find a differential equation for the gauge-invariant phase differences alone. This is done by using the general result,

$$\frac{4\pi d}{c} J_{n,n+1} = \int_{nd}^{(n+1)d} dz [\nabla \times (\nabla \times \mathbf{A})]_z = \nabla_\parallel \cdot (\mathbf{A}_{\parallel,n+1} - \mathbf{A}_{\parallel,n}) - \frac{\Phi_0}{2\pi} \nabla_\parallel^2 \chi_{n,n+1}, \quad (6)$$

and combining this with (2) and (4) to arrive at,

$$\nabla_\parallel^2 \varphi_{n,n+1} + \frac{1}{\lambda_c^2} \sin \varphi_{n,n+1} + \frac{1}{(\gamma d)^2} [\sin \varphi_{n+1,n+2} - 2 \sin \varphi_{n,n+1} + \sin \varphi_{n-1,n}] = 0. \quad (7)$$

Solving this equation will give the entire solution for currents using (4) to find $J_{n,n+1}$, and the conservation law,

$$\nabla_\parallel \cdot \mathbf{J}_{\parallel,n} = J_{n,n+1} - J_{n-1,n} \quad (8)$$

to find $\mathbf{J}_{\parallel,n}$.

III. STRUCTURE OF A JOSEPHSON VORTEX IN A LAYERED SUPERCONDUCTOR

If we place a flux line directed along the layers, the singularity associated with the vortex core can be avoided by placing the center in the insulating layer between two superconducting layers (first noticed by Bulaevskii⁵²). The structure of the “core” is similar to the structure of the phase drop across a flux line in a two-dimensional Josephson junction⁵³. This well-studied problem has a solution where the phase difference across the two layers drops by 2π over a distance of the Josephson length Λ_J .⁵⁴ For the 3D layered superconductor, this length is given by $\Lambda_J = \gamma d$, and we can think of a central region γd wide and d high as the core of an in-plane vortex. Beyond this core, the flux density and currents are quite similar to that for a continuous anisotropic superconductor²⁴. The screening by z -axis currents is much weaker than that by in-plane currents, and the flux line is stretched into an ellipsoidal shape with a large width $\sim \lambda_c$ along the layers. Even though only the “core” resembles the vortex in a 2D Josephson junction, it has become common usage in the literature to label the entire flux line with this orientation a Josephson vortex.

Consider now a flux line directed along the x -axis. The general structure of this Josephson vortex was first described by Bulaevskii⁵²: The center of the vortex lies between two layers, so that there is no core with suppressed amplitude of the order parameter, while at large distances from the center the structure is similar to a conventional flux line. The phase around the vortex is not given trivially by symmetry, but is a solution to the

non-linear equations (2). The most convenient path to a quantitative solution is to separate the problem into two different scales: At large scales we can ignore the non-linearity and there is an analytical solution. At small scales the numerical solution is simplified by ignoring the screening contribution of the vector potential. Fortunately, for $\lambda_{ab}/d \gg 1$ there is a large region of intermediate scales where both approximations work well, allowing us to match the small-scale and long-scale solutions.

We consider a vortex centered between layers 0 and 1, and $y = 0$, which is defined by the limiting values,

$$\begin{aligned} \phi_n(y) &= 0, \text{ for } y \rightarrow +\infty, \\ \phi_n(y) &= \begin{cases} -\pi, & \text{for } n \geq 1, \\ \pi, & \text{for } n \leq 0, \end{cases} \text{ for } y \rightarrow -\infty. \end{aligned} \quad (9)$$

This corresponds to the following conditions for the interlayer phase difference

$$\begin{aligned} \varphi_{n,n+1} &= 0, \text{ for } y \rightarrow \pm\infty \text{ and } n \neq 0, \\ \varphi_{0,1} &= \begin{cases} 0, & \text{for } y \rightarrow +\infty, \\ -2\pi, & \text{for } y \rightarrow -\infty. \end{cases} \end{aligned} \quad (10)$$

To obtain the distributions of current and field, we first derive a useful exact equation for the magnetic field. The current components (3) and (4) can be represented as

$$J_{n,n+1} = \frac{c}{4\pi} \nabla_y B_x^{n,n+1} = -\frac{c\Phi_0}{8\pi^2 \lambda_c^2 d} \sin \varphi_{n,n+1}, \quad (11)$$

$$J_{y,n} = \frac{c}{4\pi} \nabla_n B_x^{n-1,n} = -\frac{c\Phi_0 d}{8\pi^2 \lambda_{ab}^2} \left(\nabla_y \phi_n + \frac{2\pi}{\Phi_0} A_y \right), \quad (12)$$

where $B_x^{n,n+1}$ is the average magnetic field between the layers n and $n+1$ and ∇_n is a difference operator, $\nabla_n A_n \equiv A_{n+1} - A_n$. Collecting the combination $(4\pi/c) (-\lambda_c^2 \nabla_y J_{n,n+1} + (\lambda_{ab}^2/d) \nabla_n J_{y,n})$, we obtain

$$\begin{aligned} & [1 - \lambda_c^2 \nabla_y^2 - (\lambda_{ab}^2/d^2) \nabla_n^2] B_x^{n,n+1} \\ &= \frac{\Phi_0}{2\pi d} \nabla_y (\varphi_{n+1,n} - \sin \varphi_{n+1,n}) \end{aligned} \quad (13)$$

with $\nabla_n^2 A_n \equiv A_{n+1} + A_{n-1} - 2A_n$. The difference of $\varphi_{n+1,n}$ and $\sin \varphi_{n+1,n}$ decays outside the nonlinear core and satisfies the relation

$$\sum_n \int_{-\infty}^{\infty} dy \nabla_y (\varphi_{n+1,n} - \sin \varphi_{n+1,n}) = \sum_n \varphi_{n+1,n} \Big|_{-\infty}^{\infty} = 2\pi. \quad (14)$$

Therefore, in the continuum limit the right-hand side of (13) converts into $\Phi_0 \delta(y) \delta(z)$ and (13) transforms into the usual equation for the vortex magnetic field⁵⁵

$$B_x - \lambda_c^2 \nabla_y^2 B_x - \lambda_{ab}^2 \nabla_z^2 B_x = \Phi_0 \delta(y) \delta(z), \quad (15)$$

which gives

$$B_x = \frac{\Phi_0}{2\pi \lambda_c \lambda_{ab}} K_0 \left(\sqrt{(y/\lambda_c)^2 + (z/\lambda_{ab})^2} \right). \quad (16)$$

The current densities outside the core region are also given by standard formulas for anisotropic superconductors,

$$j_y = -\frac{c\Phi_0}{8\pi^2 \lambda_c \lambda_{ab}^2} \frac{z/\lambda_{ab}}{\sqrt{y^2/\lambda_c^2 + z^2/\lambda_{ab}^2}} K_1 \left(\sqrt{\frac{y^2}{\lambda_c^2} + \frac{z^2}{\lambda_{ab}^2}} \right), \quad (17)$$

$$j_z = \frac{c\Phi_0}{8\pi^2 \lambda_c^2 \lambda_{ab}} \frac{y/\lambda_c}{\sqrt{y^2/\lambda_c^2 + z^2/\lambda_{ab}^2}} K_1 \left(\sqrt{\frac{y^2}{\lambda_c^2} + \frac{z^2}{\lambda_{ab}^2}} \right). \quad (18)$$

These results should be valid as long as the linear approximation for the sine of the phase difference is good. To find the range of applicability for this approximation we compare the last equation to (4), which gives near the vortex center,

$$\sin \varphi_{n,n+1} = -\frac{y/\gamma d}{(y/\gamma d)^2 + n^2}, \text{ for } y^2/\lambda_c^2 + z^2/\lambda_{ab}^2 \ll 1, \quad (19)$$

indicating that the linear theory breaks down at $(y/\gamma d)^2 + n^2 \sim 1$. This condition therefore sets the boundary of the nonlinear core.

The above analysis shows that the Josephson vortex is characterized by two sets of length scales. A region where the interlayer phase difference is large defines the nonlinear core of the vortex. In the z direction this region is essentially localized within the central junction and in the y direction it spreads over the Josephson length γd . At scales $|z|, |y|/\gamma \gg d$ the vortex structure is described by the anisotropic London theory. In addition, in a wide region one can neglect screening effects where the currents around the vortex decay as $1/r$, (though the current pattern is strongly stretched along the layers). Screening of the currents and magnetic field becomes important at the length scales $|z| \approx \lambda_{ab}$ and $|y| \approx \lambda_c$, which are much larger than the corresponding boundaries of the nonlinear core.

Due to this vortex structure, a quantitative analysis may be obtained with more ease by introducing an intermediate scale R_{int} , with $d < R_{\text{int}} < \lambda_{ab}$, such that at a distance from the vortex center $\sqrt{z^2 + (y/\gamma)^2} = R_{\text{int}}$ both non-linearity and screening may be ignored. One then considers separately the small-distance region $\sqrt{z^2 + (y/\gamma)^2} < R_{\text{int}}$ (containing the nonlinear core) and the large-distance region $\sqrt{z^2 + (y/\gamma)^2} > R_{\text{int}}$ (where screening will become important). At small distances one can neglect screening. In the London gauge, $\nabla \cdot \mathbf{A} = 0$, this means that the vector potential \mathbf{A} can be dropped and the vortex is described in terms of in-plane phases $\phi_n(y)$ only, which satisfy the following equation (from (2))

$$(\gamma d)^2 \frac{d^2 \phi_n}{dy^2} + \sin(\phi_{n+1} - \phi_n) - \sin(\phi_n - \phi_{n-1}) = 0 \quad (20)$$

and the boundary conditions (9). These conditions are satisfied by our knowledge that outside the nonlinear core, $(n - 1/2)^2 + (y/\gamma d)^2 \gg 1$, the phase has to approach the scaled version of the usual form relating to

the angle around a vortex,

$$\phi_n^{\text{Jv}}(y) = -\tan^{-1}\left(\frac{\gamma d(n-1/2)}{y}\right). \quad (21)$$

Multiplying (20) by $d\phi_n/dy$, summing over n , and performing an indefinite integral over y , we derive the following exact relation for all y ,

$$\sum_n \left[(\gamma d)^2 \left(\frac{d\phi_n}{dy} \right)^2 - 2(1 - \cos(\phi_{n+1} - \phi_n)) \right] = \text{const}, \quad (22)$$

which is analogous to the first integral of a second-order differential equation with one variable. For the case of an isolated Josephson vortex the constant is zero. In contrast to the single-variable case, this relation does not help us to find the exact solution of the coupled nonlinear equations (20), and one has either to use some approximate solution or to solve it numerically. Relation (22) can, however, be used to test the accuracy of the approximate and numerical solutions.

A simple approximate solution has been proposed by Clem and Coffey⁵⁵ (the CC solution) who used the following ansatz for the magnetic field

$$B_x \approx \frac{\Phi_0}{2\pi\lambda_c\lambda_{\text{ab}}} K_0 \left(\frac{\sqrt{y^2 + \gamma^2 z^2 + y_{\text{cc}}^2}}{\lambda_c} \right). \quad (23)$$

and found that the best approximation for the core structure is achieved by selecting the cut off $y_{\text{cc}} = \gamma d/2$. This field distribution allows one to obtain the distribution of the phase difference

$$\varphi_{n,n+1} \approx -\sin^{-1} \left\{ \frac{d}{\lambda_{\text{ab}}} \frac{y}{R_n(y)} K_1 \left(\frac{R_n(y)}{\lambda_c} \right) \right\}, \quad (24)$$

where $R_n(y) = \sqrt{y^2 + (\gamma d n)^2 + y_{\text{cc}}^2}$. In particular, at $\gamma d \ll y \ll \lambda_c$, this corresponds to $\phi_1(y) \approx -\tan^{-1}(\gamma d/2y)$.

The accurate numerical structure for the core was obtained in Ref. 56. Figure 2 presents a visualization of this numerical solution, and we compare the phase difference in the central junction to that from the CC solution in figure 3. The numerical solution is characterized by the following properties. The maximum in-plane phase gradient is given by

$$\gamma d \left. \frac{d\phi_1}{dy} \right|_{y=0} = 1.10 \quad (25)$$

(the CC solution gives $\gamma d (d\phi_1/dy)_{y=0} = 2$) and the maximum Josephson current flows at a distance $y_{\text{max}} = 0.84\gamma d$ from the vortex center (the CC solution gives $y_{\text{max}} = y_{\text{cc}} = 0.5\gamma d$). The maximum magnetic field in the vortex core is given by

$$B_x^{0,1}(y=0) \approx \frac{\Phi_0}{2\pi\lambda_c\lambda_{\text{ab}}} [\ln(\lambda_{\text{ab}}/d) + 1.03]. \quad (26)$$

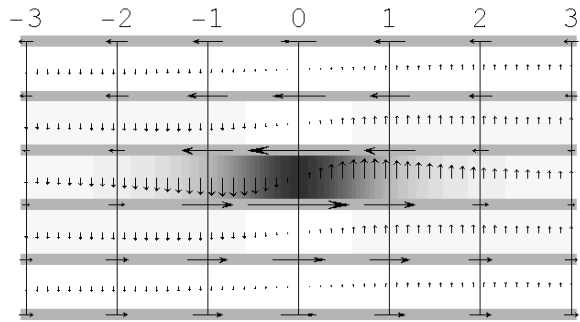


FIG. 2. Visualization of the numerically computed structure of an isolated Josephson vortex. The arrows represent the current distribution (half interlayer distance corresponds to maximum Josephson current). The greylevel codes for the cosine of the interlayer phase difference. The scale in the y -direction is in units of the Josephson length $\Lambda_J = \gamma d$.

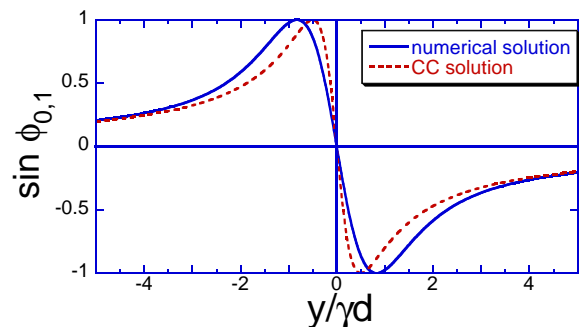


FIG. 3. Sine of the phase difference between the central layers of the Josephson vortex. For comparison, the approximate solution of Clem and Coffey⁵⁵ is also shown.

The asymptotic limits for the phase difference in the central junction are,

$$\varphi_{0,1} = \begin{cases} -\pi + \frac{2.20y}{\gamma d}, & \text{for } |y| \ll \gamma d, \\ -\frac{\gamma d}{y}, & \text{for } \gamma d \ll y \ll \lambda_c, \\ -\frac{d}{\lambda_{\text{ab}}} \sqrt{\frac{\pi\lambda_c}{2y}} e^{-y/\lambda_c}, & \text{for } \lambda_c \ll y. \end{cases} \quad (27)$$

Outside the core one can calculate the correction $\delta\phi_n(y)$ to the continuum-limit phase asymptotics (21) by treating the discreteness and nonlinearity of the Josephson current perturbatively (see appendix B). This gives

$$\delta\phi_n(y) = \frac{\sin[2\phi_n^{\text{Jv}}(y)]}{16R^2} (\ln R + C_{\delta\phi}) + \frac{5\sin[4\phi_n^{\text{Jv}}(y)]}{96R^2}, \quad (28)$$

where $R = \sqrt{(n-1/2)^2 + (y/\gamma d)^2}$, and the constant $C_{\delta\phi} \approx 4.362$ is found from comparison with the numerical solution.

We can find the energy per unit length of the Josephson vortex by inserting this solution into (1). The simplest method⁵⁶ is again to split the energy into two contributions: one from the region at large distances where the

linear approximation is valid, and one from small distances where we need the numerical solution, but can ignore the contributions of \mathbf{A} to the current (i.e. ignore screening). The first is found analytically, while the second needs a numerical integration. The final result is (see also⁵⁷),

$$\varepsilon_{\text{JV}} = \frac{\varepsilon_0}{\gamma} [\ln(\lambda_{\text{ab}}/d) + 1.55]. \quad (29)$$

with $\varepsilon_0 = \Phi_0^2/(4\pi\lambda_{\text{ab}})^2$. This energy determines the lower critical field $H_{c1,x}$ above which Josephson vortices are generated,

$$H_{c1,x} = 4\pi\varepsilon_{\text{JV}}/\Phi_0 = \frac{\Phi_0}{4\pi\lambda_c\lambda_{\text{ab}}} \ln(0.44\lambda_{\text{ab}}/d). \quad (30)$$

To summarize, the solution for a Josephson vortex presented here is very similar to the usual flux lines in isotropic superconductors, but stretched by the factor γ in the y -direction. The reason for this similarity is that the linear approximation to the Josephson relation works well away from the vortex center. The important feature, however, is that at the center of the vortex there is no normal core, but rather a phase drop of nearly 2π across the central junction over a distance of γd .

A. Line-tension energy of Josephson vortex

In this section we consider the line-tension energy of a distorted Josephson vortex, an important parameter which determines thermal wandering of the vortex line and its response to pinning centers. We consider a kink-free vortex located in between the layers 0 and 1 and defined by the planar displacement field $u(x)$. As the energy of the straight vortex does not depend on its orientation inside the layer's plane, for very smooth distortions with the wavelength larger than λ_c the line-tension energy is simply determined by the line energy (29),

$$\delta F = \int dx \frac{\varepsilon_{\text{JV}}}{2} \left(\frac{du}{dx} \right)^2 \quad \text{for } |du/dx| < |u/\lambda_c|$$

This simple result, however, has a limited interest, because most properties of the vortex are determined by deformations with smaller wavelength, $|du/dx|/|u| \sim |k_x| \gg 1/\lambda_c$. In this range, the line-tension energy acquires nonlocality, a typical feature of vortex lines. An accurate calculation of the line tension for this regime presented in Appendix A leads to the following result

$$\delta F = \frac{\pi}{2} \varepsilon_{\text{J}} \int \frac{dk_x}{2\pi} k_x^2 \ln \frac{C_t}{\gamma dk_x} u^2 \quad (31)$$

with $\varepsilon_{\text{J}} \equiv E_0/\gamma d$ and $C_t \approx 2.86$. The important feature is the logarithmic dependence of the efficient line tension on the deformation wave vector, which is a consequence of nonlocality.

IV. DILUTE LATTICE, $B_x < \Phi_0/2\pi\gamma d^2$

When the Josephson vortices are well separated, the linear and continuous approximation can be applied to the energy functional (1) everywhere except in the core regions, which reduces it to the anisotropic London model

$$F_{\text{L}}[\phi(\mathbf{r}), \mathbf{A}(\mathbf{r})] \approx \int d^3r \left\{ \frac{B_x^2}{8\pi} + \frac{E_0}{2} \left[\left(\nabla_{\parallel} \phi + \frac{2\pi}{\Phi_0} \mathbf{A}_{\parallel} \right)^2 + \frac{1}{\gamma^2} \left(\nabla_z \phi + \frac{2\pi}{\Phi_0} A_z \right)^2 \right] \right\}. \quad (32)$$

This means that the lattice solution is just a linear addition of single flux-line solutions and the lattice energy is determined by this London model. To understand the nature of the ground state it is useful to apply the rescaling trick^{58,59},

$$\tilde{\mathbf{r}} = (y, \gamma z) \quad \text{and} \quad \tilde{\mathbf{A}} = (A_y, A_z/\gamma), \quad (33)$$

which in the case of zero z -component of the magnetic field precisely reduces the system to the isotropic state²⁴. Therefore the ground state configuration in scaled coordinates is given by a regular triangular lattice. In real coordinates this state corresponds to the triangular lattice strongly stretched along the direction of the layers.

Within the anisotropic London model the lattice is degenerate with respect to rotation in scaled coordinates. In real coordinates this corresponds to an ‘‘elliptic rotation’’ illustrated in figure 4. In particular, there are two aligned configurations, in which Josephson vortices form vertical stacks along the z axis (see figure 5). For these configurations the vertical distance between the Josephson vortices in the stacks, a_z , and the separation between the stacks, a_y , are given by

$$a_z = \sqrt{\beta\Phi_0/(\gamma B_x)}, \quad a_y = \sqrt{\gamma\Phi_0/(\beta B_x)} \quad (34)$$

where the constant β is equal to $2\sqrt{3}$ and $2/\sqrt{3}$ for the upper and lower configuration in figure 5 respectively.

The interaction energy of the Josephson vortex lattice can be reduced to interaction energy of Abrikosov vortex lattice using scaling trick. This energy must be added to the self energy of each Josephson vortex (29) which, in the intermediate field regime $H_{c1,x} \ll \bar{B}_x \ll B_{\gamma d^2}$, gives the result

$$f_{\text{JL}} \approx \frac{\bar{B}_x^2}{8\pi} + \frac{\bar{B}_x}{\Phi_0} \frac{\varepsilon_0}{2\gamma} \ln \left(\frac{1.23\Phi_0}{\gamma d^2 \bar{B}_x} \right). \quad (35)$$

The ‘‘elliptic rotation’’ degeneracy is eliminated by the layered structure of superconductor. There are several different mechanisms of this elimination. First, due to the strong intrinsic pinning, the vortex centers must be located in between the layers. This limits the possible lattice orientations. A second, less trivial, mechanism is from the corrections due to the discrete lattice structure to the vortex interactions. The degeneracy is also

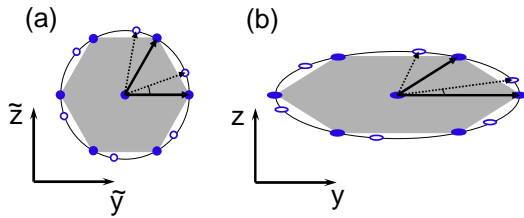


FIG. 4. Ground-state lattice configuration for an in-plane field and its rotational degeneracy within the anisotropic London model in (a) scaled coordinates and (b) real coordinates. The ellipse aspect ratio corresponds to the anisotropy factor ≈ 3 , much smaller than the anisotropy of, e.g., BSCCO.

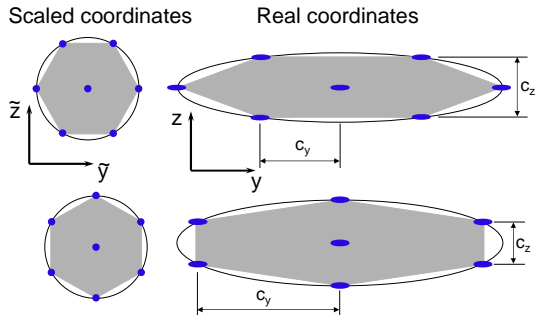


FIG. 5. The two alternative lattice configurations that are aligned with the layers, in scaled and real coordinates.

eliminated by thermal fluctuations, because the Josephson vortices mostly fluctuate along the layers directions and this selects preferential lattice orientations. All these mechanisms will be considered in details below.

A. Selection of ground-state configurations by layered structure

As the centers of the Josephson vortices must be located between the layers, the layered structure plays a crucial role in the selection of the ground-state lattice configurations. The Josephson-vortex lattice is commensurate with the layered structure only at a discrete set of magnetic fields. Due to the “elliptic rotation” degeneracy of the lattice within the London approximation, the family of commensurate lattices includes lattices aligned with the layers (see Fig. 5), as well as misaligned ones. To make a full classification of commensurate lattices we consider a general lattice as shown in Fig. 6a^{60,61}. The lattice is characterized by three parameters: the in-plane period a , the distance between vortex rows in the z direction $b = Nd$, and the relative shift between the neighboring vortex rows in qa . The lattice shape is characterized by the two dimensionless parameters, q and the ratio $r = b/a$. The lattice parameters are related to the in-plane magnetic field, B_x , as $B_x = \Phi_0/(ab)$. The two aligned structures in Fig. 5 correspond to $q = 1/2$. As the replacement $q \rightarrow 1 - q$ corresponds to a mirror re-

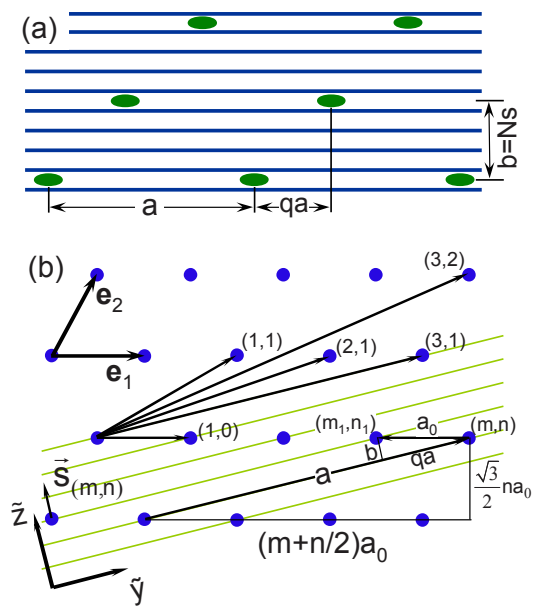


FIG. 6. (a) General Josephson vortex lattice and its parameters. (b) Orientation of layered structure with respect to ideal lattice (in scaled coordinates). The layered structure fits the ideal lattice only if it is oriented along one of the crystallographic directions, which is characterized by two numbers (m, n) , corresponding to expansion of the direction vector over the two basic lattice vectors, \mathbf{e}_1 and \mathbf{e}_2 . Several possible directions are shown with the corresponding indices (m, n) . The layers, together with the lattice parameters, a , b , and q , are drawn here for the $(3, 1)$ orientation.

flexion with respect to the x - z plane, every structure with $q \neq 1/2$ is doubly degenerate. In addition to giving the general ground states, these lattices describe multiple metastable states with unique properties studied in Refs. 60 and 61, which we will review below.

We now classify the exactly commensurate lattices to give the set of commensurate fields. An equivalent geometrical analysis has been done in Ref. 62 following a somewhat different line of reasoning, but with the same final result for the commensurate fields. The analysis of commensurability conditions can be done most conveniently in scaled coordinates (33). In these coordinates the ground-state configuration corresponds to a regular triangular lattice with period $\tilde{a}_\Delta = \sqrt{2\gamma\Phi_0}/\sqrt{3}B_x$. It is convenient to consider the orientation of the layered structure with respect to this lattice rather than the other way round. The layered structure fits this lattice only if it runs along one of the crystallographic directions, see Fig. 6b. This direction, (m, n) , is defined by the lattice vector, $\mathbf{e}_{(m,n)}$, which can be expanded over the two basic lattice vectors, $\mathbf{e}_{(m,n)} = m\mathbf{e}_1 + n\mathbf{e}_2$. For nonequivalent directions m and n must be relatively prime numbers (i.e., there is no integer other than one that divides into both m and n). Any such direction corresponds to a set of matching fields which we notate as $B_{(m,n)}(N)$. We also notate the lattice parameters corresponding to such

an orientation as $a_{(m,n)}$, $b_{(m,n)}$, and $q_{(m,n)}$. Immediately, we obtain

$$a_{(m,n)} = e_{(m,n)} = \tilde{a}_\Delta \sqrt{m^2 + mn + n^2}. \quad (36)$$

It is useful to write the unit vector perpendicular to the layers, $\hat{\mathbf{z}}$, in terms of $\mathbf{e}_{(m,n)}$. This vector is labelled $\mathbf{s}_{(m,n)}$ in Fig. 6b, and is given by,

$$\mathbf{s}_{(m,n)} \equiv \hat{\mathbf{z}} = \frac{\mathbf{e}_{(m,n)} \times \hat{\mathbf{x}}}{e_{(m,n)}}. \quad (37)$$

Commensurability means that the projections of the two basic lattice vectors on $\mathbf{s}_{(m,n)}$ should be an integer number of layers, i.e.,

$$\mathbf{e}_1 \cdot \mathbf{s}_{(m,n)} = \tilde{n}\gamma d, \quad \mathbf{e}_2 \cdot \mathbf{s}_{(m,n)} = \tilde{m}\gamma d, \quad (38)$$

(in scaled coordinates the interlayer distance is γd). Using (36) and (37), we rewrite these conditions as

$$\frac{\sqrt{3}}{2} \tilde{a}_\Delta \frac{n}{\sqrt{m^2 + mn + n^2}} = \tilde{n}\gamma d, \quad (39)$$

$$\frac{\sqrt{3}}{2} \tilde{a}_\Delta \frac{m}{\sqrt{m^2 + mn + n^2}} = \tilde{m}\gamma d. \quad (40)$$

These equations mean that $\tilde{m}/\tilde{n} = m/n$. As m and n are by definition relatively prime numbers, the set of allowed \tilde{m} and \tilde{n} is simply given by $\tilde{m} = Nm$ and $\tilde{n} = Nn$. Therefore we can represent the commensurability condition as

$$\frac{\sqrt{3}}{2} \tilde{a}_\Delta = N \sqrt{m^2 + mn + n^2} \gamma d, \quad (41)$$

which gives the following set of commensurate fields, distances between neighboring rows $b = Nd$ and ratios $r_{(m,n)}$

$$B_{(m,n)}(N) = \frac{\sqrt{3}}{2} \frac{\Phi_0}{N^2 \gamma d^2 (m^2 + mn + n^2)}, \quad (42)$$

$$b_{(m,n)} = \frac{\frac{\sqrt{3}}{2} \tilde{a}_\Delta}{\sqrt{m^2 + mn + n^2}}, \quad (43)$$

$$r_{(m,n)} = \frac{\sqrt{3}/2}{m^2 + mn + n^2}. \quad (44)$$

Finding the parameter $q_{(m,n)}$ for a general orientation is a more complicated problem. Defining the direction to the nearest-row site (m_1, n_1) (see figure 6), we have

$$q_{(m,n)} = \frac{\mathbf{e}_{(m,n)} \cdot \mathbf{e}_{(m_1, n_1)}}{|\mathbf{e}_{(m,n)}|^2} = \frac{|mm_1 + (m_1n + mn_1)/2 + nn_1|}{m^2 + mn + n^2}. \quad (45)$$

Expressing the neighboring-row separation via (m_1, n_1) ,

$$b_{(m,n)} = \frac{|\mathbf{e}_{(m,n)} \times \mathbf{e}_{(m_1, n_1)}|}{e_{(m,n)}} = \frac{\frac{\sqrt{3}}{2} \tilde{a}_\Delta |m_1n - mn_1|}{\sqrt{m^2 + mn + n^2}}$$

and comparing it with Eq. (43), we can see that pair (m_1, n_1) must satisfy the condition

$$|m_1n - mn_1| = 1. \quad (46)$$

It is well-known from the theory of numbers that for any relatively prime pair (m, n) one can find a complementary pair (m_1, n_1) satisfying this condition, and there is a general recipe to find complementary pairs based on the Euclid algorithm (see, e.g., Ref. 63). Moreover, as the combination $m_1n - mn_1$ does not change with the substitution $m_1 \rightarrow m_1 + m$, $n_1 \rightarrow n_1 + n$, there is an infinite set of pairs which satisfy condition (46) (physically, this corresponds to different lattice sites in the neighboring row). Therefore, the problem to find $q_{(m,n)}$ can be formulated as follows: among all pairs (m_1, n_1) satisfying condition (46) one must find the pair which minimizes $|mm_1 + (m_1n + mn_1)/2 + nn_1|$ and use this pair in Eq. (45). (Practically, we need not search to very high-order directions.) In the case $n = 1$ and arbitrary m the choice of (m_1, n_1) is obvious, $(m_1, n_1) = (-1, 0)$, and we obtain

$$q_{(m,1)} = \frac{m + 1/2}{m^2 + m + 1}. \quad (47)$$

We should stress that these results essentially rely on the linear London approximation, which implies a very strong inequality $\tilde{a}_\Delta \gg \gamma d$, or equivalently, $N\sqrt{m^2 + mn + n^2} \gg 1$. The number of vortex-free layers per unit cell is given by $N - 1$. The case $N = 1$ represents a special situation when all the layers are filled with vortices and are equivalent. It is interesting to note that even for a dilute lattice one can have Josephson vortices in every layer ($N = 1$) in the case of high-order commensurability ($m, n \gg 1$). In an ideal situation, the lattice transfers with changing magnetic field between different commensurate configurations via a series of first-order phase transitions. The number of competing states rapidly increases as the field decreases.

A full analysis of the structural evolution requires consideration of the energy. In the London limit a very useful expression for the energy of the general lattice in Fig. 6a has been derived in Ref. 60. We outline this derivation and present the final result in a somewhat different form. For the lattice in Fig. 6a the interaction energy in the London limit is given by,

$$f_{\text{Jl}}^{\text{int}} = \frac{B_x^2}{8\pi} \left[\sum_{l,k} \frac{1}{1 + \lambda_{\text{ab}}^2 \left[\gamma^2 (2\pi l)^2 / a^2 + [2\pi(k - ql)]^2 / b^2 \right]} - \int dy dz \frac{1}{1 + \lambda_{\text{ab}}^2 \left[\gamma^2 (2\pi z)^2 / a^2 + (2\pi y)^2 / b^2 \right]} \right]$$

Using the formula

$$\sum_{k=-\infty}^{\infty} \frac{1}{(k+v)^2 + u^2} = \frac{\pi}{u} \frac{\sinh(2\pi u)}{\cosh(2\pi u) - \cos(2\pi v)}$$

we can sum over k and integrate over y leading to

$$f_{\text{Jl}}^{\text{int}} = \frac{B_x^2}{8\pi} \frac{b^2}{2\pi\lambda_{\text{ab}}^2} \left[\frac{\pi\lambda_{\text{ab}}}{b} \frac{\sinh(b/\lambda_{\text{ab}})}{\cosh(b/\lambda_{\text{ab}}) - 1} + \sum_{l=1}^{\infty} \frac{1}{g_b(l)} \frac{\sinh[2\pi g_b(l)]}{\cosh[2\pi g_b(l)] - \cos(2\pi ql)} - \int_0^\infty dz \frac{1}{g_b(z)} \right]$$

with $g_b(z) = \sqrt{(b/2\pi\lambda_{ab})^2 + r^2 z^2}$ and $r = b\gamma/a$. This expression significantly simplifies in the intermediate region $b \ll 2\pi\lambda_{ab}$, where we can use the expansion

$$\frac{\pi\lambda_{ab}}{b} \frac{\sinh(b/\lambda_{ab})}{\cosh(b/\lambda_{ab}) - 1} \approx \frac{2\pi\lambda_{ab}^2}{b^2} + \frac{\pi}{6}$$

and drop $b^2/(2\pi\lambda_{ab})^2$ in $g_b(z)$ meaning that $g_b(z) \rightarrow rz$. This allows us to represent the interaction energy in this regime as⁶⁰

$$f_{\text{JI}}^{\text{int}} = \frac{B_x^2}{8\pi} + \frac{B_x\Phi_0}{(4\pi)^2\lambda_{ab}\lambda_c} \times \left[\frac{1}{2} \ln \left(\frac{\Phi_0}{2\pi\lambda_{ab}\lambda_c B_x} \right) + \gamma_E - \ln 2 + G_L(r, q) \right] \quad (48)$$

with $\gamma_E = 0.5772$ being the Euler constant and

$$G_L(r, q) = \frac{\pi r}{6} + \sum_{l=1}^{\infty} \frac{\cos(2\pi ql) - \exp(-2\pi rl)}{l[\cosh(2\pi rl) - \cos(2\pi ql)]} - \frac{1}{2} \ln(2\pi r). \quad (49)$$

The dimensionless function $G_L(r, q)$ depends only on the lattice shape. Its absolute minimum corresponding to the triangular lattice is given by $G_L(\sqrt{3}/2, 1/2) = -0.4022$. A peculiar property of the function $G_L(r, q)$, following from the rotational degeneracy, is that it also has this value for the whole set of pairs $(r, q) = (r_{(m,n)}, q_{(m,n)})$ corresponding to the different lattice orientations. In particular, for $(m, n) = (m, 1)$ we have $G_L\left(\frac{\sqrt{3}/2}{m^2+m+1}, \frac{m+1/2}{m^2+m+1}\right) = G_L(\sqrt{3}/2, 1/2)$. This function also has very peculiar behavior at small r which is important for the statistics of metastable states⁶¹: at $r \rightarrow 0$ it acquires peaks at all rational values of $q = k/l$. Large-order peaks with denominator l develop as r drops below $1/(2\pi l)$.

For layered superconductors we have

$$b = Nd, \quad a = \frac{\Phi_0}{B_x d N}, \quad r = N^2 \frac{B_x}{B_{\gamma d^2}}$$

with $B_{\gamma d^2} = \Phi_0/(\gamma d^2)$ and, adding the energy of isolated Josephson vortices, we can write the total energy of the lattice as

$$f_{\text{JI}}(N, q, h) = \frac{B_x^2}{8\pi} + \frac{B_x\Phi_0}{(4\pi)^2\lambda_{ab}\lambda_c} \left[\frac{1}{2} \ln \left(\frac{1}{h} \right) + 1.432 + G_L(r, q) \right] \quad (50)$$

with $h \equiv 2\pi B_x/B_{\gamma d^2}$ and $r = N^2 h/2\pi$. For given h the ground state configuration is determined by the minimum of $G_L(N^2 h/2\pi, q)$ with respect to discrete N and continuous q . As follows from Eq. (42), perfect fits where G_L reaches its absolute minimum occur at the set of reduced fields $h = h_{(m,n)}(N)$ with

$$h_{(m,n)}(N) = \frac{\sqrt{3}\pi}{N^2(m^2 + mn + n^2)}. \quad (51)$$

At these fields this energy reproduces the result (35). The field dependence of G_L for the ground state is shown in Fig. 9. The continuous London model does not accurately describe layered superconductors at high fields. To obtain lattice structures in this region one has to consider the more general Lawrence-Doniach model. The transition between the *aligned* lattices have been studied within this model by Ichioka⁶⁴. However, our analysis in the next section shows that at many fields the true ground state is not given by an aligned lattice.

B. Evolution of ground-state configurations within Lawrence-Doniach model

The accurate analysis of the lattice configurations within the Lawrence-Doniach model which we report in this section was only published in short Proceeding⁶⁵. Independently, such numerical analysis was done by Nonomura and Hu⁶⁶ with fully consistent results.

At high in-plane magnetic fields the spatial variations of the field are very small and in the first approximation can be neglected. In this limit the only relevant degrees of freedom are the superconducting phases and the relevant part of the LLD energy (1) per unit volume, $f_\phi \equiv F_{\text{LLD}}/(L_x L_y L_z) - B_x^2/(8\pi)$, can be written as

$$f_\phi[\phi_n(\mathbf{r})] = \frac{E_0}{L_y L_z} \sum_n \int dy \left[\frac{1}{2} (\nabla_y \phi_n)^2 + \frac{1}{(\gamma d)^2} \left(1 - \cos \left(\phi_{n+1} - \phi_n + \frac{2\pi d B_x y}{\Phi_0} \right) \right) \right]. \quad (52)$$

To simplify the analysis we will introduce the reduced in-plane length $\bar{y} \equiv y/\gamma d$ and the reduced magnetic field $h \equiv 2\pi\gamma d^2 B_x/\Phi_0$ leading to

$$f_\phi[\phi_n(\mathbf{r})] = \frac{\varepsilon_J}{L_y L_z} \sum_n \int d\bar{y} \left[\frac{1}{2} (\nabla_{\bar{y}} \phi_n)^2 + 1 - \cos(\phi_{n+1} - \phi_n + h\bar{y}) \right] \quad (53)$$

with $\varepsilon_J \equiv E_0/\gamma d$. Varying this energy with respect to the phases $\phi_n(\bar{y})$ we obtain an equation for the equilibrium phase distribution [equivalent to (2) when we ignore the spatial dependence in B_x]

$$\nabla_{\bar{y}}^2 \phi_n + \sin(\phi_{n+1} - \phi_n + h\bar{y}) - \sin(\phi_n - \phi_{n-1} + h\bar{y}) = 0. \quad (54)$$

We again consider a general lattice shown in Fig. 6a with in-plane period a , N layers between neighboring rows, and relative shift qa between relative rows with a and N being related to the reduced field as $h = 2\pi\gamma d/Na$. It is sufficient to find the solution for the phase in one unit cell, $0 < y < a$, $1 \leq n \leq N$, using appropriate quasi-periodicity conditions for the phase. The total lattice energy per unit volume can be represented as

$$f_\phi = \frac{B_x\Phi_0}{(4\pi)^2\lambda_{ab}\lambda_c} u(N, q, h), \quad (55)$$

where the reduced energy $u(N, q, h)$ per unit cell is given by

$$u(N, q, h) = \frac{1}{\pi} \sum_{n=1}^N \int_0^a d\bar{y} \left[\frac{1}{2} \left(\frac{d\phi_n}{d\bar{y}} \right)^2 + 1 - \cos(\phi_{n+1} - \phi_n + h\bar{y}) \right]. \quad (56)$$

Using a relaxation method to solve (54) numerically within one unit cell, we can find the energy u for any given values of N , q and h . To match the London representation (48), we write $u(N, q, h)$ in the form

$$u(N, q, h) = \frac{1}{2} \ln \frac{1}{h} + 1.4323 + G(N, q, h) \quad (57)$$

where the function $G(N, q, h)$ defined by this equation approaches the London limit $G_L(r = N^2 h / 2\pi, q)$ for $h \rightarrow 0$.

We consider first influence of the layered structure at small fields. As shown in the appendix B, in the lowest order with respect to h the layered structure gives orientation-independent correction to energy, $G \approx (h/32) \ln(C_h/h)$. In higher (quadratic) order the layered structure generates orientation-dependent correction to the lattice energy leading to a break down of the ‘‘elliptic-rotation’’ degeneracy of the lattice. To study this effect quantitatively we plotted in Fig. 7 the computed field dependencies of $G(N, q, h)$ for several lattice orientations at the corresponding reduced commensurate fields $h_{(m,n)}(N)$ given by (51). At small h , $h < 0.05$, neglecting a very weak dependence on orientation, one can accurately fit the correction from the layeredness as

$$G(h) - G_L \approx \frac{h}{32} \ln \frac{110}{h} - 0.075h^2. \quad (58)$$

One can see that among the two aligned structures shown in Fig. 5 the layers favor the lower structure with indices (1, 1). However, for $h < 0.1$ the energy difference between the two structures is tiny and in real samples external factors may select the lattice orientation. On the other hand, one can expect that at sufficiently large fields the ground-state configuration will be selected by the layered structure even in real samples.

Energy corrections due to the layered structure favor lattice stretching along the layer direction and shift down the matching fields. This effect is strongest for the aligned lattice (1,0) and is illustrated in Fig. 8. In this figure we show the field dependences of $G(N, h, 0.5)$ for different N . When a smooth function is subtracted from these dependences, local minima are realized at fields $\tilde{h}_{(1,0)}(N)$ which are smaller than the London matching field $h_{(1,0)}(N)$. The shift $\tilde{h}_{(1,0)}(N) - h_{(1,0)}(N)$ rapidly decreases with increasing magnetic field. We found that this shift is described by the following equation

$$\tilde{h}_{(1,0)}(N) \approx \frac{h_{(1,0)}(N)}{1 + (0.63/N^2) \ln(19/\tilde{h}_{(1,0)}(N))}.$$

For other lattice orientations the shift is smaller but still noticeable. To quantify the energy difference between the aligned lattices due to the layered structure, we fit their energies at the *shifted* matching field for $h < 0.1$ to smooth curves and subtract these curves. This procedure gives $G_{(1,1)} - G_{(1,0)} \approx -0.011h^2$.

We can now explore the evolution of the ground-state configuration by direct minimization of the energy with respect to the lattice parameters N and q as defined in Fig. 6. To this end we have computed the reduced ground-state energy defined as $G(h) \equiv \min_{N,q} [G(N, q, h)]$. We checked that if we consider only aligned lattices, the results of Ichioka⁶⁴ are reproduced for the transition fields between lattices with different periods N in the case of large anisotropy. For comparison, we also made a similar calculation for the London model and computed the field dependence of the function $G_L(h) = \min_{N,q} [G_L(r = N^2 h / (2\pi), q)]$ where $G_L(r, q)$ is defined in Eqs. (48) and (49). In figure 9 we compare field evolutions of these ground-state reduced energies and the corresponding c -axis period N . For clearer comparison we subtracted from $G(h)$ its fitted correction from $G_L(\sqrt{3}/2, 1/2)$ at small h given in (58). Values of the London commensurate fields $h_{(m,n)}(N)$ are shown on the top axis with several low-order fields being marked by corresponding indices using the format $(m, n)_N$. As expected, $G_L(h)$ reaches its absolute minimum for every $h_{(m,n)}(N)$. We can observe several interesting properties. As the lattice orientation with indices $(m, n) = (1, 0)$ is not favored by the layered structure, several low- N configurations, $3 \leq N \leq 6$, expected at $h = h_{(1,0)}(N)$, are skipped. However, as one can see from the inset in Fig. 10, for $N = 5$ and 6 the ground-state energy is smaller than the energies of these states at $h = h_{(1,0)}(N)$ only by a tiny value. For $h < 0.2$ the actual evolution of lattice structure starts to follow roughly the London route (except for skipped state $(1, 0)_6$ near $h = 0.16$) but with small negative offset, i.e., we again see that the matching fields systematically shifted down in comparison with their London values.

The field dependence of the energy function $G(N, q, h)$ in an extended field range is shown in figure 10 for the ground state and competing states. Each curve corresponds to the minimum of $G(N, q, h)$ with respect to q at fixed h and N and is marked by its value of N . We also show the first six lattice configurations which are realized with decreasing field. The inset of the figure blows up the low-field region. One can see that many lattice configurations compete for the ground state at small fields and at several fields (e.g., at $h \approx 0.19, 0.137, 0.105 \dots$) one or more lattice configurations have energies very close to the ground-state energy. We also note that there are several extended field ranges where in the ground state all layers are homogeneously filled with vortices ($N = 1$) even in the region of the dilute vortex lattice, e.g., $0.115 < h < 0.17$, $0.21 < h < 0.38$.

We see that an accurate consideration within both London and Lawrence-Doniach models shows that the

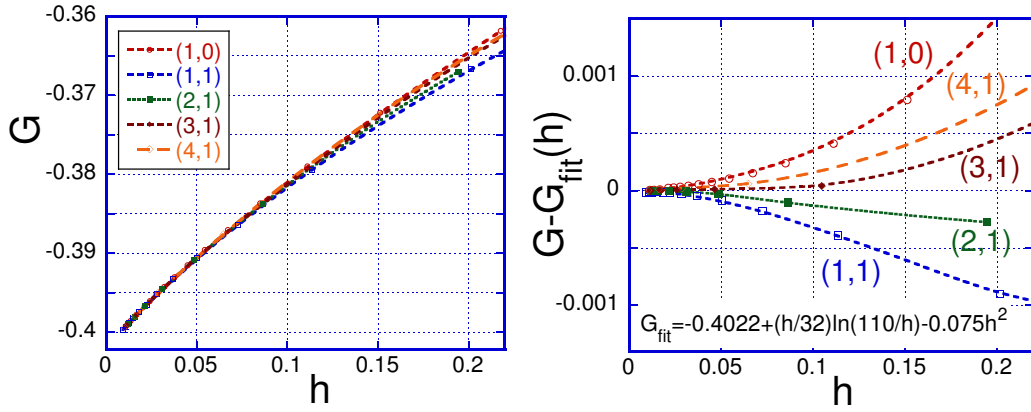


FIG. 7. Left panel: Field dependence of the reduced-energy function $G(N, h, q)$ for several lattice orientations (m, n) at the commensurate field $h_{(m,n)}(N)$. To enlarge small differences, we plot in the right panel the difference between G and its fit obtained using all data for $h < 0.05$.

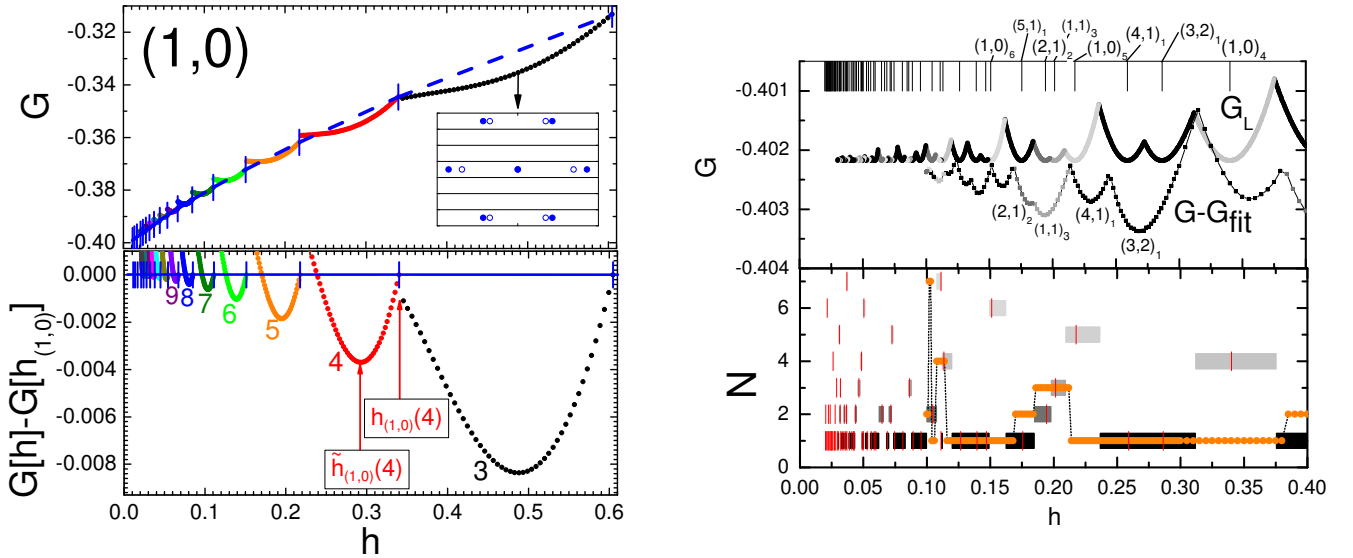


FIG. 8. *Upper panel*: The field dependences of the reduced-energy function $G = G(N, h, 0.5)$ for the aligned lattice $(1,0)$ and different N . Vertical bars mark locations of the London-model commensurate fields $h_{(1,0)}(N)$. *Lower panel* shows difference between $G(N, h, 0.5)$ and smooth curve through the points $(h_{(1,0)}(N), G(N, h_{(1,0)}(N), 0.5))$ (dashed line in the upper panel). One can see that the matching fields systematically displaced to the lower values $\tilde{h}_{(1,0)}(N)$, as illustrated for $N = 4$. Inset in the upper panel shows lattice structure at the displaced matching field for $N = 3$ (solid symbols) in comparison with the regular-hexagon structure at the London matching field.

ground state of the Josephson vortex lattice at low temperatures does not give any preference to the lattices aligned with the layers. Therefore for equilibrium field dependencies one can not expect to observe

FIG. 9. *Upper panel*: The field dependence of the reduced energy functions for London model (G_L , upper curve) and full Lawrence-Doniach model ($G - G_{\text{fit}}$, lower curve). For clearer comparison we subtracted from $G(h)$ its fit at small h given by Eq. (58). Values of commensurate fields $h_{(m,n)}(N)$ are shown in the top axis and the corresponding indices for several of them are written in the format $(m, n)_N$. As expected, G_L reaches its absolute minimum for every $h_{(m,n)}(N)$. The *lower panel* shows field dependence of N for ground state for both models (stripes for the London model and circles for the Lawrence-Doniach model). The same graylevel codes the value of N in the upper panel and the London-model plot in the lower panel.

any strong features at the matching fields of these lattices, $B_{(1,0)}(N)$ and $B_{(1,1)}(N)$ given by Eq. (43). Nevertheless, clear commensurability oscillations have been observed experimentally in underdoped YBCO in irre-

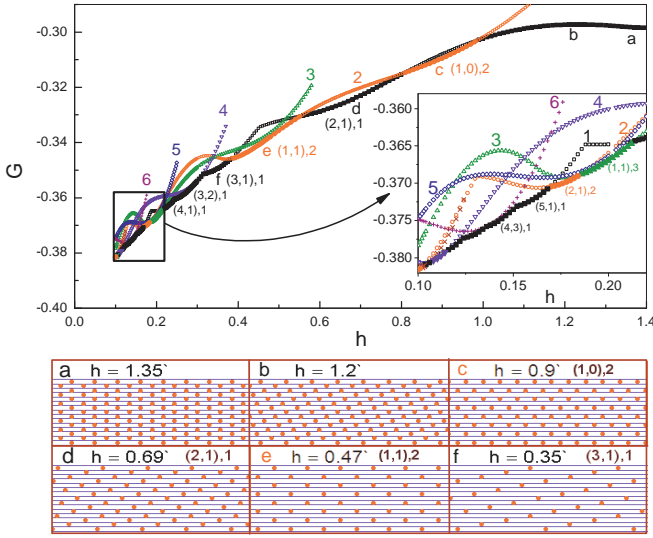


FIG. 10. Field dependence of the energy function $G(N, q, h)$ for the ground state and competing states. Each curve corresponds to the minimum of $G(N, q, h)$ with respect to q at fixed h and N . The curves are marked by the value of N . Lattice configurations in scaled coordinates are shown at six marked fields. Inset illustrates competition between different configuration at smaller fields

versible magnetization^{29,30} and nonlinear resistivity³¹. The period of these oscillations corresponds to the fields $B_{(1,0)}(N)$ indicating that for some reason in this material the aligned lattice (1, 0) occurs to be preferable. We note that, due to small differences between the energies of different configurations, in real materials aligned lattices can be selected by external factors, such as interaction with correlated disorder (twin boundaries or dislocations) or sample surface. We will also see that the aligned lattice with indices (1, 0) is favored by thermal fluctuations. Finally, we mention the work of Ikeda and Isotani⁶⁷ who performed similar analysis of the ground state configurations for field applied along the layers within the *lowest Landau level approximation*.

C. Properties of metastable states in London model

Josephson vortices can slide easily along the layers but there is a huge barrier for the motion across the layers. This property makes it hard to equilibrate the lattice. It also leads to the appearance of a very large number of metastable states. The properties of these states have been considered in Refs. 60 and 61. Systematically, metastable states at fixed c-axis period can be sampled by first slowly cooling down the superconductor at fixed magnetic field and then in a second step decreasing the magnetic field at a low temperature⁶¹. We assume that the prepared starting configuration is the *aligned* lat-

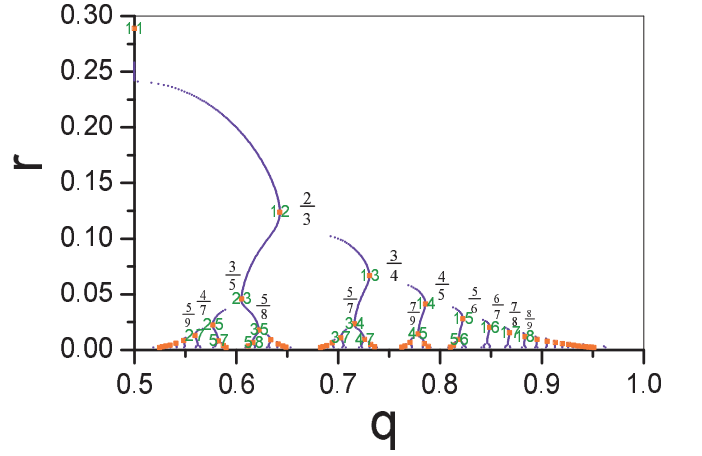


FIG. 11. Levitov's hierarchical plot of metastable states in q - r plane⁶¹ (in this plot q is selected within the interval $[0.5, 1]$). Each dotted curve is obtained from the local minima of function $G_L(r, q)$ with respect to q at fixed r . New branches appear as a result of “quasi-bifurcations”. Each “quasi-bifurcation” is associated with a rational number. The branches turn at points $(q_{(m,n)}, r_{(m,n)})$ corresponding to ground states (marked by squares and labelled by the indices mn in the plot).

tice. As the c-axis period, N , is locked by the layers, the lattice stretches along the layers with lowering the field, i.e., the ratio $r = b/a$ decreases. During stretching, these fixed- N metastable states go through a sequence of nontrivial structural transformations. In the London regime, the aligned configuration becomes unstable at $r_0 \approx 1.51/(2\pi) \approx 0.24$ ⁶⁰. This instability is driven by the repulsion between neighboring vortices in the vertical stack. At low $r < r_0$ the parameter q continuously decreases starting from $1/2$ to lower values. We found that the layeredness stabilizes the aligned structures: the critical ratio decreases to 0.231 at $N = 3$ and to 0.224 at $N = 2$. It is important to note that the shear instability occurs *in the ground state* only for $N = 1$ (we consider in detail this structural phase transition below). At higher values of N this instability only occurs when the state for this given N is metastable with respect to other values of N . This instability is considered in detail below.

The statistics of metastable states has been explored in detail in Ref. 61 where the similarity to the phyllotaxis phenomenon in biological systems has been pointed out. For every r one can find all local minima, $q_i(r)$ of the energy function $G(r, q)$ with respect to q and plot all these minima in the q - r plane (see Fig. 11). The obtained pattern is quite peculiar. At $r > r_0$ the only minimum is at $q_0(r) = 1/2$. Below $r = r_0$ this trajectory symmetrically splits into two. With further decrease of r many more minima appear forming a complex hierarchical structure. The pattern can be viewed as a series of “quasi-bifurcations” occurring near rational values of q . “Quasi-bifurcation” corresponds to the appearance of a new branch below a certain value of r in the vicin-

ity of the old branch. The branches turn at the points $(q_{(m,n)}, r_{(m,n)})$ corresponding to ground states. The evolution of the initial state is described by the two main trajectories symmetrically split from $q = 1/2$. The trajectory with $q > 1/2$ “quasi-bifurcates” at $q = F_j/F_{j+1}$ where F_j are the Fibonacci numbers and approaches the “golden ratio” $(\sqrt{5} - 1)/2 \approx 0.618$ as $r \rightarrow 0$. It goes through ground states with the indices also described by the Fibonacci sequence, $(m, n) = (F_{j+1}, F_j)$. Unfortunately, these exciting predictions have never been verified experimentally because there is no direct way to probe the structure of the Josephson vortex lattice.

D. Elasticity of dilute Josephson vortex lattice

Josephson vortices easily slide along the layers but motion across the layers is strongly suppressed by intrinsic pinning from the layers. Due to the intrinsic pinning, z axis fluctuations of the vortex lines occur via kink formation. In moderately anisotropic layered superconductors, such as YBCO, in which the c -axis coherence length is larger than or comparable with the interlayer spacing d , the intrinsic pinning potential $V(u_z)$ can be described as a cosine function of z axis vortex displacements $V(u_z) = -V_0 \cos(2\pi u_z(x)/d)$. However such description becomes inadequate in strongly layered materials, where the structure of a kinks is very similar to the structure of a pancake vortex.

In strongly layered materials at low temperatures one can neglect kink formation and take into account only in-plane lattice deformations $u(\mathbf{r}) \equiv u_y(\mathbf{r})$ (planar-fluctuations model). In this case, one can derive the following nonlocal elastic energy in the k -space

$$F_{el} = \frac{1}{2} \int \frac{d^3\mathbf{k}}{(2\pi)^3} [c_{11}(\mathbf{k})k_y^2 + c_{44}(\mathbf{k})k_x^2 + c_{66}k_z^2] |u(\mathbf{k})|^2 \quad (59)$$

with elastic moduli

$$c_{66} = \frac{B_x \Phi_0}{(8\pi)^2 \lambda_c^2 \gamma}, \quad (60)$$

$$c_{11}(\mathbf{k}) = \frac{B_x^2/4\pi}{1 + \lambda_{ab}^2 k_z^2 + \lambda_c^2 (k_y^2 + k_x^2)} - \frac{B_x \Phi_0}{(8\pi)^2 \lambda_{ab} \lambda_c}, \quad (61)$$

$$c_{44}(\mathbf{k}) = \frac{B_x^2/4\pi}{1 + \lambda_{ab}^2 k_z^2 + \lambda_c^2 (k_y^2 + k_x^2)} + \frac{B_x \Phi_0}{(4\pi)^2 \lambda_{ab} \lambda_c} \ln \frac{1}{s \sqrt{c_z^{-2} + (\gamma k_x/\pi)^2}}. \quad (62)$$

While the tilt $[c_{44}(\mathbf{k})]$ and compression $[c_{11}(\mathbf{k})]$ moduli are not sensitive to exact lattice structure, the formula for the shear modulus c_{66} is valid only for perfect matching between the Josephson vortex lattice and layered structure, which is achieved at matching fields (42). For a general lattice shown in Fig. 6a one can derive a more general expression for c_{66} using representation (48)–(49)

for the lattice energy⁶⁰ and relation between lattice deformation and change of parameter q , $\delta q = r du/dz$,

$$c_{66} = \frac{B_x \Phi_0}{(8\pi)^2 \lambda_c^2 \gamma} g_{66}(r, q) \quad (63)$$

with

$$g_{66}(r, q) = 4r^2 \frac{\partial^2}{\partial q^2} G_L(r, q) = -(4\pi)^2 r^2 \times \sum_{l=1}^{\infty} \frac{\cos(2\pi ql) \cosh(2\pi rl) - \sin^2(2\pi ql) - 1}{(\cosh(2\pi rl) - \cos(2\pi ql))^3} l \sinh(2\pi rl).$$

This formula reproduces the result (60) for the commensurate configurations $(r, q) = (r_{(n,m)}, q_{(n,m)})$. It also describes instability of aligned configuration ($q = 1/2$) at $r \approx 0.24$ ⁶⁰.

Softest mode in the planar model corresponds to shearing between neighboring planar arrays of Josephson vortices. The harmonic approximation breaks for this mode first. The simplest extension of the linear elastic energy which describes strong interplanar fluctuation is amounts to replacement of the continuous displacement field $u(\mathbf{r})$ by displacement of the planar arrays $u_j(x, y) \equiv u(x, y, jb)$ and replacement the shear term in the energy by the non-linear interaction term

$$\int d^3\mathbf{r} \frac{c_{66}}{2} \left(\frac{du}{dz} \right)^2 \rightarrow \int d^2\mathbf{r} \frac{a^2 c_{66}}{(2\pi)^2 b} \sum_j \left[1 - \cos \left(2\pi \frac{u_{j+1} - u_j}{a} \right) \right]$$

Such extension has been used to study strong-fluctuations region⁶⁸.

V. DENSE LATTICE, $B_x > \Phi_0/2\pi\gamma d^2$

With increasing magnetic field distance between Josephson vortices decreases and at field $B \sim B_{cr} = \Phi_0/2\pi\gamma d^2 = B_{\gamma d^2}/2\pi$ this distance becomes of the order of the vortex-core size. In contrast to the Abrikosov vortex lattice, for which overlap of the vortex cores marks disappearance of superconductivity, for the Josephson vortex lattice this field just marks a crossover to a new regime, the dense Josephson vortex lattice. Existence of this regime was pointed out by Bulaevskii and Clem²⁵. In the dense Josephson vortex lattice the gauge invariant phase difference is a smoothly increasing function of distance and the Josephson coupling energy can be treated as a small perturbation. This allows for the following quantitative description.

A. Very high fields: Quantitative description using expansion in Josephson coupling

At high fields $B_x > B_{cr}$, vortices homogeneously fill all of the layers. This means that all layers are equivalent

and the in-plane lattice period is $\tilde{a} = 2\pi/h$ (see figure 12). When the strong inequality $B_x \gg B_{cr}$ ($h \gg 1$) is satisfied Eq. (54) for the phases can be solved using an expansion with respect to the Josephson currents. In the zeroth order we can construct a regular lattice with an arbitrary translation from layer to layer by using the form,

$$\phi_n^{(0)} = \kappa \frac{n(n-1)}{2}.$$

This corresponds to the gauge-invariant phase difference

$$\varphi_{n,n+1}^{(0)} = \kappa n + h\bar{y},$$

i.e., the planar lattices in the neighboring layers are shifted by the fraction $q = \kappa/2\pi$ of the in-plane lattice spacing \tilde{a} . In the first order we obtain

$$\nabla_{\bar{y}}^2 \phi_n^{(1)} + \sin(\kappa n + h\bar{y}) - \sin(\kappa(n-1) + h\bar{y}) = 0$$

which gives

$$\phi_n^{(1)}(\bar{y}) = \frac{1}{h^2} [\sin(\kappa n + h\bar{y}) - \sin(\kappa(n-1) + h\bar{y})].$$

Substituting this solution into (53), we obtain the energy per unit volume up to second order with respect to the Josephson coupling,

$$f_\phi(\kappa, h) = \frac{\varepsilon_J}{\gamma d^2} \left(1 - \frac{1 - \cos \kappa}{2h^2} \right). \quad (64)$$

We can immediately see that the minimum energy $f_{\min}(h) = (\varepsilon_J/\gamma d^2)(1 - 1/h^2)$ is achieved at $\kappa = \pi$, corresponding to the triangular lattice shown in figure 12. The phase distribution in the ground state is given by

$$\phi_n(\bar{y}) \approx \pi \frac{n(n-1)}{2} + \frac{2(-1)^n}{h^2} \sin(h\bar{y}) \quad (65)$$

From this solution we can recover the distributions of the in-plane and Josephson current

$$j_{y,n}(y) \approx -\frac{2(-1)^n}{h} \gamma j_J \cos\left(\frac{2\pi d B_x y}{\Phi_0}\right),$$

$$j_{z,n}(y) \approx -(-1)^n j_J \sin\left[-\frac{4(-1)^n}{h^2} \sin\left(\frac{2\pi d B_x y}{\Phi_0}\right) + \frac{2\pi d B_x y}{\Phi_0}\right],$$

and a weak modulation of the in-plane field

$$B_x(y) \approx B_x - \frac{(-1)^n \Phi_0^2}{B_x (2\pi d \lambda_c)^2} \cos\left(\frac{2\pi d B_x y}{\Phi_0}\right).$$

A schematic distribution of the currents is shown in figure 12.

B. Dense lattice close to the crossover region. Structural phase transition

When the magnetic field approaches the crossover field $\Phi_0/(2\pi\gamma d^2)$, the perturbative approach of the previous

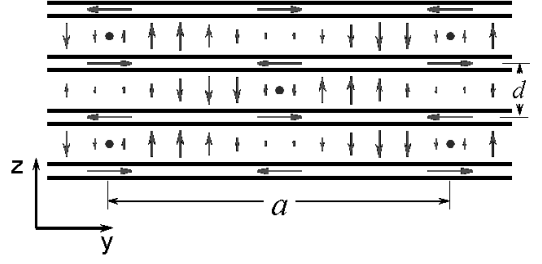


FIG. 12. Schematic distribution of currents in the dense Josephson vortex lattice. The circles mark the centers of the Josephson vortices.

section becomes insufficient and one has to obtain a full solution of the nonlinear equation (54). The general solution for the lattice with the arbitrary phase shift κ can be written as

$$\phi_n(\bar{y}) = \kappa \frac{n(n-1)}{2} + g\left(\bar{y} + \frac{\kappa n}{h}\right), \quad (66)$$

where $g(\bar{y})$ is a periodic function, $g(\bar{y} + 2\pi/h) = g(\bar{y})$, which obeys the following equation

$$\frac{d^2 g}{d\bar{y}^2} + \sin\left(g\left(\bar{y} + \frac{\kappa}{h}\right) - g(\bar{y}) + h\bar{y}\right) - \sin\left(g(\bar{y}) - g\left(\bar{y} - \frac{\kappa}{h}\right) + h\bar{y} - \kappa\right) = 0. \quad (67)$$

The reduced energy $\bar{f} \equiv f_\phi \gamma d^2 / \varepsilon_J$ can also be written in terms of the function $g(\bar{y})$,

$$\bar{f} = \int_0^{2\pi/h} \frac{hd\bar{y}}{2\pi} \left\{ \frac{1}{2} \left(\frac{dg}{d\bar{y}} \right)^2 + 1 - \cos\left[g\left(\bar{y} + \frac{\kappa}{h}\right) - g(\bar{y}) + h\bar{y}\right] \right\}. \quad (68)$$

Equation (67) does not have an analytical solution and has to be solved numerically. Lattice configurations of the dense lattice also has been investigated using the code developed for the lattice with general period N . Both approaches give identical results. Numerical investigation shows that the triangular lattice with $\kappa = \pi$ gives the ground state for $h > 1.332$. At $h \approx 1.332$ the system has a second-order phase transition to a lattice of lower symmetry, see lattice structures for $h = 1.35$ (a) and $h = 1.2$ (b) in figure 10. The field dependence of κ and corresponding lattice shift q are shown in figure 13. Ikeda and Isotani⁶⁷ found that within the lowest Landau level approximation this structural phase transition occurs at somewhat higher value, $h \approx 1.4$.

To study validity range of the high- h approximation of the previous section we plot in figure 14 the computed field dependence of the reduced energy together with its high-field asymptotics, derived in the previous section. As one can see, the perturbative approach gives a good approximation for the energy down to $h \sim 2$.

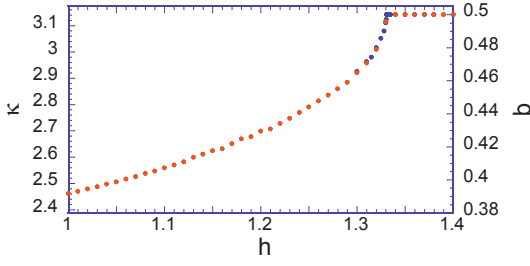


FIG. 13. Field dependence of the phase shift κ and corresponding lattice shift q for the dense Josephson vortex lattice. At $h \approx 1.332$ the lattice experiences a continuous structural phase transition.

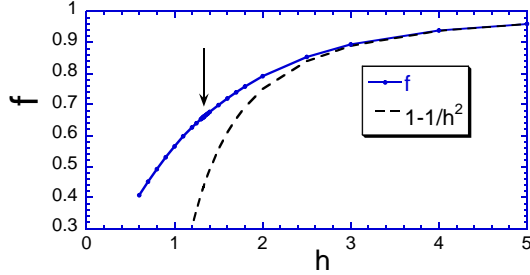


FIG. 14. Field dependence of the reduced energy for the dense Josephson vortex lattice. The dashed line shows the high-field asymptotics. The arrow marks the position of the structural phase transition at $h \approx 1.332$.

C. Elasticity of dense lattice

In this section we consider the deformation energy of the dense Josephson vortex lattice in the limit $h = 2\pi\gamma d^2 B_x / \Phi_0 \gg 1$. In particular, this energy serves as a starting point for analysis of fluctuations. We will follow the approach used by Korshunov and Larkin⁶⁹. The starting point of the analysis is again reduced LLD energy in the phase approximation (53) which we rewrite now for the general case of the phase depending on both reduced coordinates $\bar{\mathbf{r}} \equiv (\bar{x}, \bar{y}) = \mathbf{r}/\gamma d$,

$$F_\phi = E_0 \sum_n \int d^2\bar{\mathbf{r}} \left[\frac{1}{2} \left(\frac{d\phi_n}{d\bar{\mathbf{r}}} \right)^2 - \cos(\phi_{n+1} - \phi_n + h\bar{y}) \right]. \quad (69)$$

The ground-state phase distribution is given by Eq. (65). Now we consider small deformations of the lattice and split the total phase into the smooth (v_n) and rapidly oscillating in the y direction ($\tilde{\phi}_n$) parts

$$\phi_n(\bar{\mathbf{r}}) = \pi \frac{n(n+1)}{2} + v_n(\bar{\mathbf{r}}) + \tilde{\phi}_n(\bar{\mathbf{r}}), \quad (70)$$

where we assume $dv_n/d\bar{y} \ll v_n$ and $\tilde{\phi}_n \ll 1$. As the smooth part of the gauge-invariant phase difference is given by $h(\bar{y} + (v_{n+1} - v_n)/h) + \pi n$, the quantity $u_n = -(v_{n+1} - v_n)/h$ represents a local lattice displacement. Substituting representation (70) in the en-

ergy (69), expanding with respect to $\tilde{\phi}_n$, and dropping rapidly-oscillating terms, we obtain

$$F_\phi \approx E_0 \sum_n \int d\bar{\mathbf{r}} \left[\frac{1}{2} \left(\frac{d\tilde{\phi}_n}{d\bar{y}} \right)^2 + \frac{1}{2} \left(\frac{dv_n}{d\bar{\mathbf{r}}} \right)^2 + (\tilde{\phi}_{n+1} - \tilde{\phi}_n) \sin(v_{n+1} - v_n + h\bar{y} + \pi n) \right]. \quad (71)$$

As $\tilde{\phi}_n$ rapidly oscillates only in y direction, we kept only its \bar{y} derivative. Minimization of this energy with respect to $\tilde{\phi}_n$ gives

$$\tilde{\phi}_n \approx (-1)^n \frac{\sin(v_{n+1} - v_n + h\bar{y}) + \sin(v_n - v_{n-1} + h\bar{y})}{h^2}.$$

Substituting this solution into Eq. (71) and averaging with respect to \bar{y} , we finally obtain the coarse-grained energy of the deformed dense Josephson vortex lattice⁶⁹, which we write in real units

$$F_\phi \approx \frac{E_0}{2} \sum_n \int d\mathbf{r} \left[\left(\frac{dv_n}{d\mathbf{r}} \right)^2 - \frac{\cos(v_{n-1} + v_{n+1} - 2v_n) + 1}{(\Lambda_J h)^2} \right]. \quad (72)$$

This energy describes the phase fluctuations in large in-plane magnetic field. The first term is just usual in-plane phase stiffness energy. In the elasticity-theory language this term represents the compression (dv_n/dy) and tilt (dv_n/dx) contributions. The second term represents the shearing interactions between the Josephson vortex arrays in neighboring junctions. It originates from the Josephson coupling energy and can be viewed as the effective Josephson coupling renormalized by the in-plane magnetic field. Roughly, we can state that with increasing magnetic field the effective Josephson energy decreases as $1/h^2$ and the effective Josephson length, $\Lambda_J h$, increases linearly with h ,

$$\Lambda_J h = \Lambda_J h = \frac{2\pi\gamma^2 d^3 B_x}{\Phi_0}. \quad (73)$$

In the case of slowly-changing from layer to layer deformation, we can expand cosine in Eq. (72) and obtain the harmonic elastic energy of the dense Josephson vortex lattice in terms of smooth phase deformations

$$F_{\phi-el} \approx \frac{E_0}{2} \sum_n \int d\mathbf{r} \left[\left(\frac{dv_n}{d\mathbf{r}} \right)^2 + \frac{(v_{n-1} + v_{n+1} - 2v_n)^2}{2(\Lambda_J h)^2} \right] \quad (74)$$

$$= \frac{E_0}{2d} \int \frac{d^2\mathbf{k}_\parallel}{(2\pi)^2} \int_{-\pi/d}^{\pi/d} \frac{dk_z}{2\pi} \left[k_\parallel^2 + \frac{2(1 - \cos k_z d)^2}{(\Lambda_J h)^2} \right] |v^k|^2 \quad (75)$$

Using relation between the phase perturbation and lattice displacements

$$v^k = -\frac{hu^k}{\Lambda_J (\exp(ik_z d) - 1)},$$

we can rewrite the elastic energy in a more traditional way, via lattice deformations

$$F_{\phi-el} = \frac{1}{2} \int \frac{d^2\mathbf{k}_\parallel}{(2\pi)^2} \int_{-\pi/d}^{\pi/d} \frac{dk_z}{2\pi} \left[c_{11}(k_z) k_\parallel^2 + c_{66} \tilde{k}_z^2 \right] |u^k|^2 \quad (76)$$

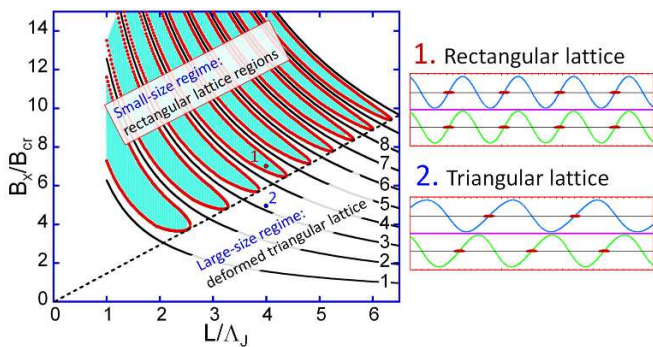


FIG. 15. Size-magnetic field phase diagram of the confined Josephson-junction stack. Dashed line separates the large-size and small-size regimes. Black lines correspond to integer flux quanta per junction. Shaded areas mark regions of rectangular-lattice ground state. Representative lattice configurations in two points are illustrated by plots of oscillating Josephson currents in two neighboring layers. Small ellipses mark the centers of the Josephson vortices.

with elastic constants

$$c_{11}(k_z) = \frac{B_x^2}{4\pi} \frac{1}{\tilde{k}_z^2 \lambda_{ab}^2}; \quad c_{66} = \frac{\Phi_0^2}{32\pi^3 d^2 \gamma^4 \lambda_{ab}^2}$$

where we used notation $\tilde{k}_z \equiv 2 \sin(k_z d/2)/d$. Note that in our case the nonlocal tilt modulus $c_{44}(k_z)$ is identical to compression modulus $c_{11}(k_z)$ and they coincide with elastic moduli within the anisotropic London model (61) and (62) in the limit $\tilde{k}_z \lambda_{ab} \gg 1, k_x \lambda_z$. This elastic energies (74), (75), and (76) can be used to study weak fluctuations and weak pinning of the dense Josephson vortex lattice. The shear modulus is field independent in the dense-lattice regime. One can check that it matches the dilute-lattice result (60) at the crossover field.

D. Lattice configurations and magnetic oscillations in finite-size samples

In this section we consider dense-lattice configurations in finite-size samples. This study is actually motivated by experimental observations of magnetic oscillations in small-size BSCCO mesas with lateral sizes 2-20 μm ⁴⁵⁻⁴⁹. Such small-size mesas behave as stacks of intrinsic Josephson junctions with strong inductive coupling between the neighboring junctions. The detailed analytical theory describing the magnetic field dependences of lattice configurations and critical current has been developed in Refs. 70. Lattice structures also have been extensively explored numerically^{46,48,71,72} and both approaches give identical results. In a small-size sample the lattice structure is determined by two competing interactions: the interaction with boundaries that favors an aligned rectangular configuration and the bulk shearing interaction between neighboring layers which favors a triangular configuration. Depending on the mesa

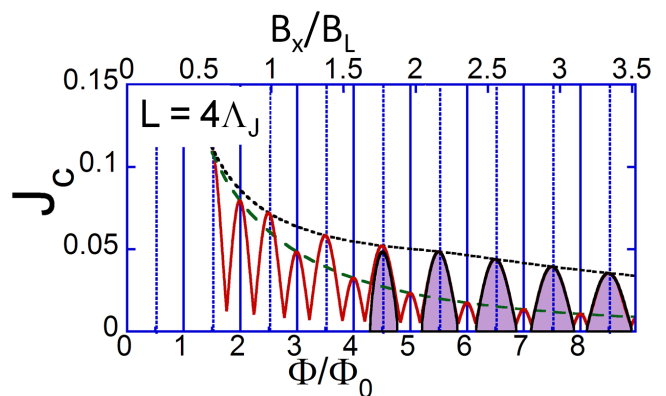


FIG. 16. Illustration of the oscillating magnetic field dependence of the critical current for $L = 4\Lambda_J$. Crossover between $\Phi_0/2$ and Φ_0 periodicity is seen at $h\bar{L} = B_x/B_L \sim 1$. Shaded areas show the regions of stable rectangular lattice.

width L and magnetic field, two very different regimes realize. In the large-size regime the vortex lattice is triangular and it is only deformed near the edges. In the small-size regime the lattice structure experiences a periodic series of phase transitions between rectangular and triangular configurations. The triangular configurations in this regime are realized only in narrow regions near magnetic-field values corresponding to an integer number of flux quanta per junction where the interaction with edges vanishes. The typical width of the mesa which separates these two regimes is given by the length Λ_{Jh} , Eq. (73), which is proportional to the applied magnetic field. Hence, the crossover from one regime to another is driven by the magnetic field and the corresponding crossover field scale is $B_L = B_{cr}L/\Lambda_J = L\Phi_0/(2\pi\gamma^2 d^3)$, for $B_x > B_L$ the small-size regime realizes. The size-field phase diagram is shown in Fig. 15. The regimes are characterized by distinctly different oscillating behavior of the critical current as function of the magnetic field. In the small-size regime, the critical current oscillates with the period of one flux quantum per junction, similar to a single junction. In the large-size regime, due to the triangular lattice ground state, the oscillation period is half flux quantum per junction.

The quantitative study of the described behavior is based on the reduced energy (69), which have to be rewritten for the finite-size case, $0 < \bar{y} < \bar{L} \equiv \bar{L}_y$, and also assuming that the system is uniform along the field direction, i.e., $\int d\bar{x} \rightarrow \bar{L}_x \int_0^{\bar{L}} d\bar{y}$. This energy has to be supplemented with the boundary conditions at the edges, $d\phi_n/d\bar{y} = 0$ for $\bar{y} = 0, \bar{L}$. The important parameter in the case of finite-size sample is the total magnetic flux through one junction, $\Phi = B_x dL$, which is connected with the reduced magnetic field by relation $h\bar{L} = 2\pi\Phi/\Phi_0$. In the dense-lattice limit, we again use presentation of Eq. (70) containing the smooth phase v_n , and rapidly oscillating component $\tilde{\phi}_n$. It is natural to as-

sume that the interactions with the boundaries preserve the alternating nature of the vortex lattice. In this case symmetry allows us to take the smooth phase in the form

$$v_n(\bar{y}) = \alpha n + (-1)^n v(\bar{y}) \quad (77)$$

where α describes the translational displacement of the lattice and v describes lattice deformations with respect to the triangular lattice. In particular, one can show that the maximum value of $v(\bar{y})$, $v_{\max} = \pi/4$, describes the rectangular lattice, i.e., identical ϕ_n in all layers up to 2π phase shift. The corresponding rapid phase becomes $\tilde{\phi}_n(\bar{y}) \approx (-1)^n 2 \cos(2v) \sin(\alpha + h\bar{y})/h^2$. Averaging with respect to the rapid oscillations for such $v_n(\bar{y})$, gives the reduced energy per layer and per unit length along x , $f_\phi = F_\phi \Lambda_J / (NL_x E_0)$,

$$f_\phi \approx -\frac{1}{h} [\sin(2v_0) \cos \alpha - \sin(2v_L) \cos(h\bar{L} + \alpha)] + \frac{1}{2} \int_0^{\bar{L}} d\bar{y} \left[\left(\frac{dv}{d\bar{y}} \right)^2 - \frac{1 + \cos(4v)}{h^2} \right], \quad (78)$$

in which the bulk part directly follows from Eq. (72) for general $v_n(\bar{y})$. Varying this energy with respect to $v(\bar{y})$, we obtain that it obeys the static sine-Gordon equation

$$\frac{d^2 v}{d\bar{y}^2} - \frac{2}{h^2} \sin(4v) = 0 \quad (79)$$

with the boundary conditions

$$\begin{aligned} \frac{dv}{d\bar{y}}(0) &= -\frac{2}{h} \cos(2v_0) \cos \alpha, \\ \frac{dv}{d\bar{y}}(L) &= -\frac{2}{h} \cos(2v_L) \cos(h\bar{L} + \alpha). \end{aligned} \quad (80)$$

Substituting solution of these equations into the energy functional (78) gives the energy as a function of the lattice shift α , $f_\phi(\alpha)$. Minimum of the energy with respect to α gives the ground state for given h and \bar{L} . Higher-energy states at other values of α typically carry a finite current. The total Josephson current flowing through the stack is proportional to $df_\phi/d\alpha$. Taking derivative of the functional (72) with respect to α , assuming that at every α it is minimized with respect to $v(u)$, we obtain the total current in units of $j_J \Lambda_J L_x$

$$J(\alpha) = \frac{1}{h} [\sin(2v_0) \sin \alpha - \sin(2v_L) \sin(h\bar{L} + \alpha)]. \quad (81)$$

An important consequence of this equation is that nonzero current exists only if the surface deformations v_0 and v_L are finite.

The general solution of equations (79) and (80) can be written in terms of the elliptic integrals and elaborated analytical analysis is possible⁷⁰. Here we summarize the most important results of this analysis for two limiting cases.

In the *large-size regime*, $L \gg \Lambda_{Jh}$ or $B_x \ll B_L$, the smooth alternating deformation $v(\bar{y})$ has solution in the

form of two isolated surface solitons⁷⁰. For example, near the edge $\bar{y} = 0$ such soliton solution decaying from the surface into the bulk is given by the well-known formula for the sine-Gordon kink

$$\tan v = \tan v_0 \exp\left(-2\sqrt{2}\bar{y}/h\right), \quad (82)$$

where the boundary value v_0 can be found from the boundary condition (80) leading to $\tan(2v_0) = \sqrt{2} \cos \alpha$. Using this solution, one can find the surface energy and surface current for the edge $\bar{y} = 0$ as functions of the lattice displacement α ,

$$f_s(\alpha) = \frac{1}{\sqrt{2}h} (1 - \sqrt{2 + \cos 2\alpha}), \quad (83)$$

$$j_s(\alpha) = -\frac{1}{\sqrt{2}h} \frac{\sin 2\alpha}{\sqrt{2 + \cos 2\alpha}}. \quad (84)$$

The 2α periodicity of these results is a consequence of the triangular lattice structure: the change of α by π corresponds to the vertical lattice displacement by one layer. Similar solution is realized at the opposite edge $\bar{y} = \bar{L}$. Its energy and current can be obtained from the above results using the substitution $\alpha \rightarrow \alpha + h\bar{L}$. For a wide stack one can neglect the interaction between the solitons and the total Josephson current is given by the sum of two independent surface currents,

$$J(\alpha) = j_s(\alpha) + j_s(\alpha + h\bar{L}).$$

The critical current J_c can be found as maximum of $J(\alpha)$ with respect to α giving the following result in real units

$$J_c(B) = J_J \frac{\Phi_0}{2\pi dLB_x} \mathcal{F}\left(\frac{2\pi dLB_x}{\Phi_0}\right), \quad (85)$$

where $J_J = j_J LL_x$ is the maximum Josephson current through the sample at zero field, and oscillating function $\mathcal{F}(\chi)$ has period π and in the range $0 < \chi < \pi/2$ can be approximated by the following formula, $\mathcal{F}(\chi) \approx 0.128 + 0.888 \cos(\chi) + 0.021 \cos(3\chi)$. We can see that, in this regime the product $B_x J_c$ has periodicity of half flux-quantum per junction and reaches maxima at points $\Phi = dLB_x = j\Phi_0/2$ with $B_x J_{c,\max} \approx 1.035 J_J \Phi_0 / (2\pi dL)$. This corresponds to the low-field part of the plot in Fig. 16. All other properties of the sample should also oscillate with the period of half flux quantum. Such oscillations of the flux-flow resistivity in BSCCO micro-mesas have been first detected experimentally in Ref. 45 and later confirmed by several experimental groups.

In the *small-size regime* $L < \Lambda_{Jh}$ or $B_x > B_L$ the interaction with edges dominates. As a consequence, extended regions of the rectangular lattice appear in the phase diagram, see Fig. 15. The energy of the rectangular lattice, $v = \pm\pi/4$, coincides with the well-known result for a single junction

$$f_{\text{rect}}(\alpha) = -\frac{2}{h} \sin\left(\frac{hL}{2}\right) \sin\left(\alpha + \frac{hL}{2}\right). \quad (86)$$

and has minimum $f_{\text{rect}} = -2 |\sin(hL/2)|/h$ at $\alpha = -hL/2 + \delta\pi/2$ with $\delta = \text{sign}[\sin(hL/2)]$. An accurate analysis⁷⁰ shows that the rectangular lattice is stable with respect to small deformations at $\alpha = -h\bar{L}/2 + \pi/2$ in the regions $|h\bar{L}/2\pi - (k + 1/2)| < 1/4$ only if the inequality

$$|\sin(h\bar{L}/2)| < \tan(\sqrt{2}\bar{L}/h)/\sqrt{2} \quad (87)$$

is satisfied. These regions are plotted in the phase diagram, Fig. 15. This means that the rectangular lattices first appear in the ground state at points $h\bar{L} = (k + 1/2)2\pi$ for $\bar{L}/h \leq l_1 = \arctan(\sqrt{2})/\sqrt{2} \approx 0.675$. This corresponds to the dashed line shown in the phase diagram of Fig. 15. If, however, L/h is only slightly smaller than this value, the rectangular lattice becomes unstable with increasing current and the configuration at the critical current still corresponds to the deformed lattice. The accurate analysis shows that there is another typical value of the ratio L/h , $L/h = l_2 \approx 0.484$, below which *the rectangular lattice remains stable up to the critical current*.

In the region $h \gg \bar{L}$ the rectangular lattice is realized in the most part of the phase diagram except narrow regions in the vicinity of the integer-flux quanta lines, $hL/2\pi = \Phi/\Phi_0 = k$ where the interaction with edges vanishes. Switching between the rectangular and triangular lattices in the ground state occurs via a first-order phase transition⁷⁰ at the transition fields which are determined by equation

$$\left| \sin\left(\frac{h_t \bar{L}}{2}\right) \right| = \frac{3 \bar{L}}{2 h_t}. \quad (88)$$

At high fields the critical current approaches the classical Fraunhofer dependence for a single small junction, $J_F(\Phi) = J_J |\sin(\pi\Phi/\Phi_0)|/|\pi\Phi/\Phi_0|$. Two important deviations persist at all fields and sizes: (i) Near the points $\Phi = k\Phi_0$, due the phase transitions to the triangular lattice, the critical current never drops to zero and actually always has small local maxima; (ii) Away from the points $\Phi = k\Phi_0$ the critical current is reached at the instability point of the rectangular vortex lattice and it is always somewhat smaller than the ‘‘Fraunhofer’’ value $J_F(\Phi)$.

In the region $B \sim B_L$ the crossover between the two described regimes takes place. In the oscillations of the critical current this crossover manifests itself by breaking the $\Phi_0/2$ periodicity, the maxima at the half-integer flux-quantum points $\Phi = (k + 1/2)\Phi_0$ progressively become larger while the maxima at the integer flux-quantum points $\Phi = k\Phi_0$ become smaller. This crossover behavior of the critical current is illustrated in Fig. 16. Such behavior was indeed observed experimentally in very narrow BSCCO mesas^{46,48,49}.

VI. THERMAL FLUCTUATIONS

In this section we consider thermal fluctuations effects for the Josephson vortex lattice. Confinement of the vor-

tex cores in between the layers leads to strong suppression of the vortex motion across the layers, which can only occur via formation of kinks. Therefore, as a first step, one can neglect these energy-costly displacements and consider only planar fluctuations of vortices along the layers. This simple model describes fluctuation behavior in the most part of the field-temperature phase diagram but it occurs to be insufficient for description of the melting transition of the lattice. In general, thermal effects for Josephson vortices are much weaker than for pancake-vortex lattice and phase transformations are expected only in the vicinity of the transition temperature. On the other hand, due to the intrinsic pinning potential and involvement of the kink excitations, the overall behavior near the melting line is rather complicated and, in spite of quite extensive theoretical effort^{68,69,73–77} and numerical simulations^{78,79}, there is no clear consensus on the nature of melting transition and structure of the phase diagram for magnetic field aligned with direction of the layers.

A. Thermal effects for dilute Josephson vortex lattice: problem of intermediate phase

A standard first step to study thermal fluctuation effects is to evaluate the mean-squared local fluctuation displacement from the elastic energy (59)⁸⁰

$$\langle u^2 \rangle = \int \frac{d^3 \mathbf{k}}{(2\pi)^3} \frac{T}{c_{11}(\mathbf{k})k_y^2 + c_{44}(\mathbf{k})k_x^2 + c_{66}k_z^2}. \quad (89)$$

Introducing reduced wave vector $\tilde{\mathbf{k}}$ as

$$k_x = k_{\text{BZ}} \tilde{k}_x / \sqrt{\gamma}, \quad k_y = k_{\text{BZ}} \tilde{k}_y / \sqrt{\gamma}, \quad k_z = k_{\text{BZ}} \sqrt{\gamma} \tilde{k}_z, \quad (90)$$

where $k_{\text{BZ}} = \sqrt{4\pi B_x / \Phi_0}$ is the average wave vector of the Brillouin zone, we rewrite this integral in a more explicit form.

$$\begin{aligned} \langle u^2 \rangle &= \frac{(4\pi)^2 k_{\text{BZ}} \lambda_c^2 T}{\sqrt{\gamma} \Phi_0 B_x} \int \frac{d^3 \tilde{\mathbf{k}}}{(2\pi)^3} \left[\left(\frac{1}{\tilde{k}^2} - \frac{1}{4} \right) \tilde{k}_y^2 \right. \\ &\quad \left. + \left(\frac{1}{\tilde{k}^2} + \ln \frac{b/s}{\sqrt{1 + \beta^2 \tilde{k}_x^2}} \right) \tilde{k}_x^2 + \frac{\tilde{k}_z^2}{4} \right]^{-1} \end{aligned}$$

with $\beta \sim 1$. Evaluation of this integral leads to the following result

$$\frac{\langle u^2 \rangle}{a_0^2} = \frac{0.12T}{b_0 \sqrt{\ln(b_0/d)} \varepsilon_0}, \quad (91)$$

where $a_0 = \sqrt{\gamma \Phi_0 / B_x}$ and $b_0 = \sqrt{\Phi_0 / \gamma B_x}$ are the typical lattice constant in the y and z directions. From this result one can obtain estimate for the typical temperature at which fluctuations become strong⁶⁸

$$T_f \sim b_0 \sqrt{\ln(b_0/d)} \varepsilon_0 (T_f). \quad (92)$$

Unfortunately, this temperature is located very close to T_c where one can not use approximations behind Eq. (59), e.g., neglect thermal activation of kinks and antikinks. We can conclude that *the planar-fluctuations model given by the elastic energy (59) is not sufficient to describe the melting of the Josephson-vortex lattice*⁶⁸ The temperature scale (92) is much higher than the corresponding temperature scale for the pancake vortex lattice¹⁹ meaning that thermal-fluctuation effects for the Josephson vortex lattice are much weaker than for the pancake vortex lattice.

We can estimate the typical temperature above which kink formation strongly influences the fluctuation displacements of the vortex lines. In the isolated line the typical distance between thermally excited kinks is given by

$$L_{\text{kink}} = \xi_{\text{kink}} \exp(E_{\text{kink}}/T), \quad (93)$$

where $E_{\text{kink}} \approx d\varepsilon_0 \ln(\gamma d/\xi_{\text{ab}})$ is the kink energy. Usually, it is assumed that the preexponential factor ξ_{kink} is of the order of the in-plane coherence length ξ_{ab} ⁷⁵. Analysis of fluctuations of the order parameter near the core⁸¹ gives somewhat more accurate estimate $\xi_{\text{kink}} \sim \xi_{\text{ab}} \sqrt{T/d\varepsilon_0}$. Typical k_x contributing to the fluctuation displacement (89) can be estimated as $k_x \sim \pi/b_0$. Therefore, the kinks start to contribute to thermal wandering if $L_{\text{kink}} < b_0$. This gives estimate for typical temperature

$$T_{\text{kink}} = E_{\text{kink}} / \ln(b_0/\xi_{\text{kink}}). \quad (94)$$

In the limit $\gamma > \xi_{\text{ab}}/d$, we obtain

$$T_{\text{kink}} = d\varepsilon_0(T_{\text{kink}}) \frac{\ln(\gamma d/\xi_{\text{ab}})}{\ln(b_0/\xi_{\text{kink}})}. \quad (95)$$

One can see that even though this temperature is smaller than T_f (92), it is also located close to the fluctuation region near T_c and very slowly decreases with increasing magnetic field.

The planar-fluctuations model belongs to universality class of the three-dimensional XY model meaning that the phase transition described by this model has to be continuous. In spite of insufficiency of this model, this suggests that the melting transition for the magnetic field applied along the layers may become continuous for sufficiently high anisotropy. It was indeed observed experimentally by Kwok *et al.*⁸² and by Gordeev *et al.*³¹ that the melting transition in YBCO becomes continuous when magnetic field is aligned with the layers. Continuous melting of the Josephson vortex lattice also has been observed in numerical simulations by Hu and Tachiki⁷⁸. The simulation parameters in this work, however, correspond to the regime of dense lattice, which will be considered below.

A description of the fluctuating Josephson vortices taking into account kink-antikink formation is much more complicated problem and possibilities for analytical progress are quite limited. General scenarios of

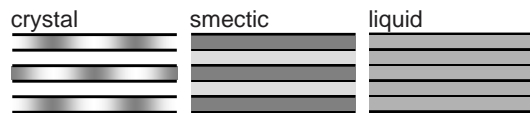


FIG. 17. Possible phases for field applied along the layers. Grey level illustrates average vortex density. In the intermediate smectic phase suggested in Ref. 75 density is modulated only in the direction perpendicular to the layers.

Josephson-vortex-lattice melting have been discussed by Balents and Nelson⁷⁵. They argued that an aligned lattice may melt via an intermediate smectic phase, in which the average vortex density is modulated only in the direction perpendicular to the layers but no order is preserved in the direction of the layers, as illustrated in Fig. 17. The period of density modulation has to be equal to the integer number of layers. The developed Landau theory of the liquid-to-smectic transition suggests that this transition has to be of the second order. Static and dynamic properties of the intermediate smectic phase have been described in detail. In particular, Balents and Nelson argued that this phase is characterized by finite but very large tilt modulus, corresponding to very small transversal susceptibility $\mu_z = B_z/H_z$, and by very small in-plane resistivity. Both these properties appear due to the thermally-activated “superkink” excitations, in which one vortex is moved across the layers by one smectic period. While the density modulation remains static and oriented parallel to the layers, these excitations may facilitate tilting of the magnetic induction with respect to the layers and flux motion in the z -axis direction. In spite of its physical appeal, the theory of Balents and Nelson is not quantitative. It does not predict locations of the transitions in the field-temperature plane, their thermodynamic signatures, and the width of the intermediate-phase region. The very existence of the intermediate smectic phase has been not rigorously proven. Alternatively, the crystal may melt directly into the liquid via a first-order phase transition.

More quantitative study based on the density-functional theory has been performed recently by Hu, Luo, and Ma⁷⁷. The intrinsic pinning potential in this study has been modeled by the cosine function and its strength has been used as an adjusting parameter. It was found that the smectic phase exists for sufficiently strong periodic potential only for one type of aligned lattice, which in our notations corresponds to $(m, n) = (1, 0)$ and with one empty layer between the layers filled with Josephson vortices, i.e., with $N = 2$. According to analysis of Sec. IV B such lattice is realized in ground state within field interval $[0.8 - 0.98]\Phi_0/(2\pi\gamma d^2)$. The melting scenario via the intermediate smectic phase is most probable in this field range.

B. Elimination of the lattice rotational degeneracy by thermal fluctuations

The dilute lattice at small field is approximately degenerate with respect to elliptic rotations, as it was discussed in Sec. IV. This degeneracy is partially eliminated by intrinsic pinning potential and by the corrections to the intervortex interactions due to discreteness of the layered structure. The latter effect becomes noticeable only at high magnetic field approaching the crossover field. As the Josephson vortices mainly fluctuate along the layer direction, the fluctuation correction to the free energy depends on the lattice orientation with respect to the layers and also eliminates the elliptic degeneracy. Therefore the Josephson vortex lattice at small fields gives a physical realization of a system in which the ground state is highly degenerate at zero temperature and this degeneracy is eliminated by thermal fluctuations. Similar behavior is realized in some frustrated magnetics and is known as “order as an effect of disorder”⁸³. As a natural way to prepare the ground state is to cool system in fixed field, it is important to understand how the ground-state configuration evolves with the temperature.

In this section we consider the orientation-dependent entropy correction to the free energy. This will allow us to trace evolution of the ground-state configurations with increasing field at finite temperature. Qualitatively, fluctuations favor soft lattices, with smaller elastic constants. One can expect then that the entropy correction favors the aligned lattice (1,0), because for this lattice the shear deformations take place along the closed-packed direction.

The orientation-dependent entropy correction is determined by the short-wavelength lattice deformations and the long-wavelength elastic approximation of the previous section is not sufficient. The elastic energy for planar deformations in the whole Brillouin zone is given by

$$F_{\text{el}} = \int \frac{d^3\mathbf{k}}{(2\pi)^3} \frac{\Phi_{\text{JVL}}(\mathbf{k})}{2} |u(\mathbf{k})|^2 \quad (96)$$

with

$$\Phi_{\text{JVL}}(\mathbf{k}) = \frac{B_x^2}{4\pi} \sum_{\mathbf{Q}} \left(\frac{(k_y - Q_y)^2 + k_x^2}{1 + \lambda_{\text{ab}}^2(k_z - Q_z)^2 + \lambda_{\text{c}}^2(k_y - Q_y)^2 + \lambda_{\text{c}}^2 k_x^2} - \frac{Q_y^2}{1 + \lambda_{\text{ab}}^2 Q_z^2 + \lambda_{\text{c}}^2 Q_y^2} \right), \quad (97)$$

where $\mathbf{Q} = (Q_y, Q_z)$ are the reciprocal-lattice vectors. The fluctuation correction to the free energy is given by

$$\delta f_T = -\frac{T}{2} \int_{-\infty}^{\infty} \frac{dk_x}{2\pi} \int_{\text{BZ}} \frac{dk_y dk_z}{(2\pi)^2} \ln \frac{C}{\Phi_{\text{JVL}}(\mathbf{k})}. \quad (98)$$

Calculation of this correction is described in detail in Appendix C. Combining result of this calculation with the London-limit presentation of the lattice interaction

energy (48), we represent the orientation-dependent part of the total free energy at finite temperature in the form

$$\delta f_a = \frac{B_x \varepsilon_0}{\Phi_0 \gamma} \left(G_L - \frac{T}{\varepsilon_0} \sqrt{\frac{\gamma B_x}{\pi \Phi_0}} g_a \right). \quad (99)$$

Numerically computed orientation-dependent correction $g_a(\theta, h)$ in the range $0.001 < h < 0.1$ is well described by

$$g_a(\theta, h) \approx g_6(h) \cos(6\theta) \text{ with } g_6(h) \approx \frac{0.01}{\sqrt{\ln(514/h)}}. \quad (100)$$

The fluctuations give the largest negative contribution for $\theta = 0$, meaning that they indeed favor the aligned lattice (1,0).

Let us compare the orientation-dependent entropy correction with the correction due to the layered structure considered in Sec. IV B. We can see that these corrections compete: the first one favors the (1,0) orientation while the second one favors the (1,1) orientation. The entropy correction decays with decreasing fields as $\sqrt{B_x}$ and always exceeds at small fields the “layeredness” correction, which decays as B_x^2 . We estimate that the “layeredness” correction exceeds the fluctuation correction when B_x exceeds the temperature-dependent field scale

$$B_{x,T} = \frac{\Phi_0}{2\pi\gamma d^2} \left[\frac{T/d\varepsilon_0}{\sqrt{\ln(C_T d\varepsilon_0/T)}} \right]^{2/3}$$

with $C_T \approx 2.6 \cdot 10^4$.

C. Fluctuations and melting of dense Josephson vortex lattice

Using elastic energy (75) we can evaluate a mean-squared fluctuation of the in-plane phase

$$\langle \phi_n^2 \rangle \approx \langle v_n^2 \rangle = \frac{dT}{E_0} \int \frac{d^2\mathbf{k}_{\parallel}}{(2\pi)^2} \int_{-\pi/d}^{\pi/d} \frac{dk_z}{2\pi} \frac{1}{k_{\parallel}^2 + \frac{8}{(\Lambda_J h)^2} s_z^4}$$

with $s_z(k_z) = \sin(k_z d/2)$ and the lattice displacement $u_n = -\Lambda_J (v_{n+1} - v_n)/h$

$$\langle u^2 \rangle = \frac{dT\Lambda_J^2}{E_0} \int \frac{d^2\mathbf{k}_{\parallel}}{(2\pi)^2} \int_{-\pi/d}^{\pi/d} \frac{dk_z}{2\pi} \frac{4s_z^2}{k_{\parallel}^2 + \frac{8}{(\Lambda_J h)^2} s_z^4}.$$

Renormalization of the effective coupling is determined by the following average

$$\langle (v_{n-1} + v_{n+1} - 2v_n)^2 \rangle = \frac{dT}{E_0} \int \frac{d^2\mathbf{k}_{\parallel}}{(2\pi)^2} \int_{-\pi/d}^{\pi/d} \frac{dk_z}{2\pi} \frac{16s_z^4}{k_{\parallel}^2 + \frac{8}{(\Lambda_J h)^2} s_z^4}.$$

All above integrals are logarithmically diverging at large k_{\parallel} . This divergency has to be cut off at $k_{\parallel} \sim 1/\xi_{\text{ab}}$. As

usual for quasi-two-dimensional systems, the weak inter-layer coupling cuts off logarithmic divergency at small k_{\parallel} . Evaluating the integrals, we obtain

$$\begin{aligned} \langle \phi_n^2 \rangle &\approx \frac{T}{2\pi E_0} \ln(\Lambda_J h / \xi_{ab}); \quad \langle u^2 \rangle \approx \frac{T \Lambda_J^2}{\pi h^2 E_0} \ln(\Lambda_J h / \xi_{ab}); \\ \langle (v_{n-1} + v_{n+1} - 2v_n)^2 \rangle &\approx 6 \langle \phi_n^2 \rangle \approx \frac{3T}{\pi E_0} \ln(\Lambda_J h / \xi_{ab}). \end{aligned}$$

Fluctuations become strong and harmonic approximation breaks down when $\langle (v_{n-1} + v_{n+1} - 2v_n)^2 \rangle \sim 1$, corresponding to $\langle \phi_n^2 \rangle \sim 1/6$ and $\langle u^2 \rangle \sim a^2/3$ with $a = \Lambda_J/h$ being the in-plane lattice constant. This gives the temperature scale

$$T_f = \frac{E_0(T_f)}{\ln(\Lambda_J h / \xi_{ab})} = \frac{\varepsilon_0(T_f) d}{\pi \ln(\Lambda_J h / \xi_{ab})}. \quad (101)$$

As $E_0(0) \gg T_c$ (typically for BSCCO $E_0(0) \sim 250 - 300K$), this temperature scale usually corresponds to temperatures close to T_c . It is somewhat lower than the corresponding temperature scale for the dilute lattice (92) and even smaller than the temperature scale for kink formation in the dilute lattice (95).

We turn now to discussion of the melting transition of the dense lattice based on the energy (72) describing weakly coupled two-dimensional systems. Behavior of such system has to be similar to layered XY model⁸⁴ and to a layered superconductor in zero magnetic field⁸⁵. In the ordered phase of such systems, below the Kosterlitz-Thouless temperature for a single layer, a weak inter-layer coupling is always relevant, can not be treated as a small perturbation, and it restores three-dimensional long-range order. The transition in such system is expected to be continuous and to occur slightly above the Berezinskii-Kosterlitz-Thouless transition of an isolated layer given by equation $T_{KT} = \pi E_0(T_{KT})/2$. This is in spite of the fact that the interplane fluctuations actually become strong at the temperature (101) which is significantly smaller than the transition temperature in the isolated layer T_{KT} .

Hu and Tachiki studied numerically melting transition of the dense lattice using the frustrated XY model⁷⁸. They claimed that the melting transition is continuous at high field and it changes to a first-order transitions when the field drops below $B = \Phi_0/2\sqrt{3}\gamma d^2 \approx 1.8\Phi_0/2\pi\gamma d^2$. It is not clear how universal is this field. In principle, it may be sensitive to the kink energy, which depends on the ratio $\gamma d/\xi_{ab}$.

Experimentally, indication of the melting transition in the dense-lattice regime was found in small-size BSCCO mesas by Latyshev *et al.*⁴⁷ exploring the temperature dependence of magnetic oscillations discussed in Sec. VD. It was found that in the field range 0.6-0.8 tesla the magnetic oscillations of the flux-flow voltage rapidly decrease with increasing temperature and are completely suppressed by thermal fluctuations at temperatures $\sim 4K$ below the transition temperature.

VII. SUMMARY

In this review we considered in detail the static properties of the Josephson vortex lattice following from the Lawrence-Doniach model in London approximation, which mostly describes properties of superconductors in terms of the distribution of the order-parameter phase. We reviewed the properties of an isolated vortex as well as the structure and energetics of the vortex lattice both in dilute and dense regimes. In addition to standard properties, our consideration includes quite subtle nontrivial effects, such as the influence of thermal fluctuations on the orientation of the vortex lattice. Note that we did not touch on dynamic properties of the lattice which has become a separate large field.

ACKNOWLEDGMENTS

AEK would like to thank L. N. Bulaevskii, M. Tachiki and X. Hu for many useful discussions of theoretical issues and Yu. I. Latyshev, I. Kakeya, T. Hatano, S. Bending, V. K. Vlasko-Vlasov, A. Tonomura, and A. A. Zhukov for discussions of relevant experimental data. AEK is supported by UChicago Argonne, LLC, operator of Argonne National Laboratory, a U.S. Department of Energy Office of Science laboratory, operated under contract No. DE-AC02-06CH11357.

Appendix A: Calculation of the nonlocal line-tension energy of a single line

For deformations with wave vectors $|k_x| \gg 1/\lambda_c$ screening effects can be neglected and the energy variation is determined by the phase part of energy, which we write using scaled in-plane coordinates, $(\bar{x}, \bar{y}) = (x/\gamma d, y/\gamma d)$,

$$\begin{aligned} \delta F \approx E_0 \sum_n \int d\bar{x} \int d\bar{y} &\left[\frac{1}{2} (\nabla_{\parallel} \phi_n)^2 - \cos(\phi_{n+1} - \phi_n) \right. \\ &\left. - \frac{1}{2} (\nabla_{\bar{y}} \phi_n^{(0)})^2 + \cos(\phi_{n+1}^{(0)} - \phi_n^{(0)}) \right], \quad (A1) \end{aligned}$$

where $\phi_n^{(0)}(\bar{y})$ is the straight-vortex solution. The phase of the deformed vortex obeys the following equation

$$\nabla_{\parallel}^2 \phi_n + \sin(\phi_{n+1} - \phi_n) - \sin(\phi_n - \phi_{n-1}) = 0 \quad (A2)$$

with the condition $\phi_1(\bar{x}, \bar{u}(\bar{x})) - \phi_0(\bar{x}, \bar{u}(\bar{x})) = \pi$ defining the vortex core and $\bar{u}(\bar{x}) = u(x)/\gamma d$. In the elastic limit, $|du/dx| \ll 1$, at distances, smaller than the typical wavelength of deformation, the phase approximately can be represented as

$$\phi_n(\bar{x}, \bar{y}) \approx \phi_n^{(0)}[\bar{y} - \bar{u}(\bar{x})].$$

On the other hand, at large distances we can use London approximation of Eq. (A2) and find the phase using

Fourier transform. This gives for the phase perturbation $\phi^{(1)}(\bar{\mathbf{k}}) = \phi(\bar{\mathbf{k}}) - \phi^{(0)}(\bar{\mathbf{k}})$

$$\phi^{(1)}(\bar{\mathbf{k}}) \approx \frac{2\pi i \bar{k}_z \bar{u}(\bar{k}_x)}{\bar{k}^2}, \quad (\text{A3})$$

with $(\bar{k}_x, \bar{k}_y, \bar{k}_z) = (\gamma dk_x, \gamma dk_y, dk_z)$ and $\bar{k}^2 = \bar{k}_x^2 + \bar{k}_y^2 + \bar{k}_z^2$. We will use this result in mixed $(\bar{k}_x, \bar{y}, \bar{z})$ -representation, which is obtained by the reverse Fourier transform of the above equations with respect to \bar{y} and \bar{z}

$$\phi^{(1)}(\bar{\mathbf{r}}, \bar{k}_x) \approx \bar{u}(\bar{k}_x) \nabla_{\bar{z}} K_0(\bar{k}_x \bar{r}). \quad (\text{A4})$$

with $\bar{\mathbf{r}} = (\bar{y}, \bar{z})$.

We split the total energy loss given by Eq. (A1) into the x -gradient and transverse parts, $\delta F = F_x + F_{zy}$. The x -gradient part,

$$F_x = \frac{E_0}{2} \sum_n \int d\bar{x} \int d\bar{y} (\nabla_{\bar{x}} \phi_n)^2,$$

can be computed by introducing intermediate scale, $1 \ll R \ll 1/\bar{k}_x$, which splits the integral into the two contributions, from small and at large distances. The contribution from $\bar{r} = \sqrt{\bar{y}^2 + \bar{z}^2} < R$, with $\bar{z} = n - 1/2$ is given by

$$F_{x,<} \approx \frac{E_0}{2} \int d\bar{x} \left(\frac{d\bar{u}}{d\bar{x}} \right)^2 \sum_n \int_{-y_n}^{y_n} d\bar{y} (\nabla_{\bar{y}} \phi_n^{(0)})^2$$

with $y_n = \sqrt{R^2 - (n - 1/2)^2}$. The quantity

$$\sum_n \int_{-y_n}^{y_n} d\bar{y} (\nabla_{\bar{y}} \phi_n^{(0)})^2 \approx \frac{\pi}{2} (\ln R + C_y)$$

is determined by exact phase distribution in the core. Using the accurate numerical solution, we estimate $C_y \approx 0.93$. The contribution from the region $r > R$ is computed using Eq. (A4),

$$\begin{aligned} F_{x,>} &\approx \frac{E_0}{2} \int d\bar{x} \int_{\bar{r}>R} d^2\bar{\mathbf{r}} (\nabla_{\bar{x}} \phi_n)^2 \\ &= \frac{E_0}{2} \int \frac{d\bar{k}_x}{2\pi} \bar{k}_x^2 |\bar{u}(\bar{k}_x)|^2 \int_{\bar{r}>R} d^2\bar{\mathbf{r}} [\nabla_{\bar{z}} K_0(\bar{k}_x \bar{r})]^2. \end{aligned}$$

Computing integral

$$\int_{\bar{r}>R} d^2\bar{\mathbf{r}} [\nabla_{\bar{z}} K_0(\bar{k}_x \bar{r})]^2 \approx \pi \left(\ln \frac{2}{\bar{k}_x R} - \gamma_E - \frac{1}{2} \right),$$

with $\gamma_E \approx 0.5772$ being the Euler constant, we obtain

$$F_{x,>} \approx \frac{\pi}{2} E_0 \int \frac{d\bar{k}_x}{2\pi} \bar{k}_x^2 \left(\ln \frac{2}{\bar{k}_x R} - \gamma_E - \frac{1}{2} \right) |\bar{u}(\bar{k}_x)|^2.$$

Combining the parts $F_{x,<}$ and $F_{x,>}$, we obtain

$$F_x = \frac{\pi}{2} E_0 \int \frac{d\bar{k}_x}{2\pi} \bar{k}_x^2 \left(\ln \frac{2}{\bar{k}_x} - \gamma_E - \frac{1}{2} + C_y \right) |\bar{u}(\bar{k}_x)|^2 \quad (\text{A5})$$

In the transverse part,

$$\begin{aligned} F_{xy} &\approx E_0 \sum_n \int d\bar{x} \int d\bar{y} \left[\frac{1}{2} (\nabla_{\bar{y}} \phi_n)^2 - \cos(\phi_{n+1} - \phi_n) \right. \\ &\quad \left. - \frac{1}{2} (\nabla_{\bar{y}} \phi_n^{(0)})^2 + \cos(\phi_{n+1}^{(0)} - \phi_n^{(0)}) \right], \end{aligned}$$

we replace $\phi_n^{(0)}(\bar{y}, \bar{z})$ with $\phi_n^{(0)}(\bar{y} - \bar{u}(\bar{x}), \bar{z})$ and represent $\phi_n(\bar{x}, \bar{y})$ as $\phi_n(\bar{x}, \bar{y}) = \phi_n^{(0)}(\bar{y} - \bar{u}(\bar{x})) + \tilde{\phi}_n(\bar{x}, \bar{y})$ where the Fourier transform of $\tilde{\phi}_n(\bar{x}, \bar{y})$ at small wave vectors is given by

$$\begin{aligned} \tilde{\phi}(\bar{\mathbf{k}}) &= 2\pi i \left(\frac{1}{\bar{k}^2} - \frac{1}{\bar{k}_y^2 + \bar{k}_z^2} \right) \bar{k}_z \bar{u}(\bar{k}_x) \\ &= -\frac{2\pi i \bar{k}_x^2}{(\bar{k}_y^2 + \bar{k}_z^2) \bar{k}^2} \bar{k}_z \bar{u}(\bar{k}_x). \end{aligned}$$

We will see that the main contribution to F_{xy} comes from the distances of the order of typical wavelength of deformations far away from the core. Therefore we can expand with respect to $\tilde{\phi}_n$ and can use linear and continuous approximation

$$F_{yz} \approx \frac{E_0}{2} \int \frac{d^3\bar{\mathbf{k}}}{(2\pi)^3} (\bar{k}_y^2 + \bar{k}_z^2) |\tilde{\phi}(\bar{\mathbf{k}})|^2.$$

Substituting $\tilde{\phi}(\bar{\mathbf{k}})$ and computing integral with respect to \bar{k}_y and \bar{k}_z , which converges at $\bar{k}_y, \bar{k}_z \sim \bar{k}_x$, we obtain

$$F_{yz} \approx \frac{\pi}{4} E_0 \int \frac{d\bar{k}_x}{2\pi} \bar{k}_x^2 |\bar{u}(\bar{k}_x)|^2. \quad (\text{A6})$$

Finally, combining (A5) and (A6), we obtain the line-tension energy of the Josephson vortex (31) which is presented already in the real coordinates and the numerical constant is given by $C_t = 2 \exp(-\gamma_E + C_y)$.

Appendix B: Discrete and nonlinear corrections to the Josephson vortex phase and energy at large distances from the core

The phase distribution in the JV core $\phi_n(y)$ obeys equation (20). We will measure the in-plane coordinate y in units of the Josephson length $\Lambda_J = \gamma d$ defining the dimensionless coordinate $\bar{y} = y/\gamma d$ and rewrite (20) in the form

$$\frac{d^2\phi_n}{d\bar{y}^2} + \sin[\phi_{n+1}(\bar{y}) - \phi_n(\bar{y})] + \sin[\phi_{n-1}(\bar{y}) - \phi_n(\bar{y})] = 0.$$

At large distances from the core, $n^2 + \bar{y}^2 \gg 1$, this equation transforms into the isotropic London equation $\nabla^2\phi = 0$. In this region $\phi_n(\bar{y})$ can be approximated by a continuous function $\phi(\bar{y}, \bar{z})$ with $n \rightarrow \bar{z}$. Using Taylor series for the difference $\phi(\bar{y}, \bar{z} + 1) - \phi(\bar{y}, \bar{z})$, we obtain,

$$\begin{aligned} &\sin[\phi(\bar{y}, \bar{z} + 1) - \phi(\bar{y}, \bar{z})] + \sin[\phi(\bar{y}, \bar{z} - 1) - \phi(\bar{y}, \bar{z})] \\ &\approx \frac{\partial^2\phi}{\partial \bar{z}^2} + \frac{1}{12} \frac{\partial^4\phi}{\partial \bar{z}^4} - \frac{1}{2} \left(\frac{\partial\phi}{\partial \bar{z}} \right)^2 \frac{\partial^2\phi}{\partial \bar{z}^2} + \dots \end{aligned}$$

Therefore, the phase equation to 4-th order in the gradient (which is small at large distances) is given by

$$\frac{\partial^2 \phi}{\partial \bar{y}^2} + \frac{\partial^2 \phi}{\partial \bar{z}^2} + \frac{1}{12} \frac{\partial^4 \phi}{\partial \bar{z}^4} - \frac{1}{2} \left(\frac{\partial \phi}{\partial \bar{z}} \right)^2 \frac{\partial^2 \phi}{\partial \bar{z}^2} = 0. \quad (\text{B1})$$

This equation can be solved iteratively. For the Josephson vortex located at $\bar{y} = 0$ in between the layers 0 and 1 the zero-order solution ϕ^0 (correct to second order in the gradients), is given by the angle $\phi^0(\bar{y}, \bar{z}) = -\tan^{-1}[(\bar{z} - 1/2)/\bar{y}]$ (note that for $\bar{z} = n$ we have $\phi^0(y/\gamma d, n) = \phi_n^{\text{Jv}}(y)$ in (21)). The first-order correction $\delta\phi^1(\bar{y}, \bar{z})$ obeys the equation

$$\begin{aligned} \nabla^2 \delta\phi^1 &= -\frac{1}{12} \frac{\partial^4 \phi^0}{\partial \bar{z}^4} + \frac{1}{2} \left(\frac{\partial \phi^0}{\partial \bar{z}} \right)^2 \frac{\partial^2 \phi^0}{\partial \bar{z}^2} \\ &= \frac{2 \sin(2\phi^0) + 5 \sin(4\phi^0)}{8 \bar{r}^4} \end{aligned}$$

where $\bar{r}^2 = \bar{y}^2 + (\bar{z} - 1/2)^2$. Using the solutions of the inhomogeneous Laplace equations

$$\begin{aligned} \nabla^2 \phi &= \frac{\sin 2\phi^0}{\bar{r}^4} \rightarrow \phi = -\frac{\sin 2\phi^0}{4\bar{r}^2} \ln \bar{r} \\ \nabla^2 \phi &= \frac{\sin 4\phi^0}{\bar{r}^4} \rightarrow \phi = -\frac{\sin 4\phi^0}{12\bar{r}^2} \end{aligned}$$

we build the solution for $\delta\phi^1(\bar{r}, \phi^0)$ and arrive at the correction

$$\delta\phi(\bar{y}, \bar{z}) = \frac{\sin(2\phi^0)}{16\bar{r}^2} (\ln \bar{r} + C_{\delta\phi}) + \frac{5 \sin(4\phi^0)}{96\bar{r}^2} + \mathcal{O}(1/\bar{r}^4). \quad (\text{B2})$$

Here we have added the solution $\sin(2\phi^0)/\bar{r}^2$ of the homogeneous Laplace equation with an unknown numerical constant $C_{\delta\phi}$. Comparison of these asymptotics with the full numerical solution gives $C_{\delta\phi} \approx 4.362$. The result (B2) is given in unscaled coordinates in (28).

In a similar way, we can derive a nonlinear/discrete correction to the energy far away from the core. The reduced energy contribution to the Josephson vortex from the region $\bar{r} < \lambda_{\text{ab}}/d$ is given by

$$\varepsilon_{\text{Jv}} = \int d\bar{y} \sum_n \left[\frac{1}{2} \left(\frac{d\phi_n}{d\bar{y}} \right)^2 + 1 - \cos(\phi_{n+1} - \phi_n) \right].$$

In the region $\bar{r} \gg 1$ we can again apply expansion with respect to small gradient along the z axis which leads us to the following result

$$\begin{aligned} \varepsilon_{\text{Jv}} &\approx \int_{1 \ll \bar{r} \ll \lambda_{\text{ab}}/d} d^2 \bar{\mathbf{r}} \left[\frac{1}{2} \left(\frac{d\phi}{d\bar{y}} \right)^2 + \frac{1}{2} \left(\frac{\partial \phi}{\partial \bar{z}} \right)^2 \right. \\ &\quad \left. - \frac{1}{24} \left(\frac{\partial^2 \phi}{\partial \bar{z}^2} \right)^2 - \frac{1}{24} \left(\frac{\partial \phi}{\partial \bar{z}} \right)^4 \right]. \end{aligned}$$

In the lowest order with respect to small gradients, this gives us the correction to the energy due to layered structure

$$\delta\varepsilon_{\text{Jv}} = -\frac{1}{24} \int_{1 \ll \bar{r} \ll \lambda_{\text{ab}}/d} d^2 \bar{\mathbf{r}} \left[\left(\frac{\partial^2 \phi^0}{\partial \bar{z}^2} \right)^2 + \left(\frac{\partial \phi^0}{\partial \bar{z}} \right)^4 \right]. \quad (\text{B3})$$

In the case of a single Josephson vortex this formula is not very useful because the integral is formally diverging at small distances and is determined by the small-distance cut off. In the case of finite vortex density, however, generalization of this equation will allow us to obtain a nontrivial correction to the vortex-lattice energy.

In the vortex-lattice case at finite in-plane field following the same reasoning we obtain the correction to the reduced energy per unit cell (56)

$$\delta u = \frac{1}{\pi} \int_{u.c.} d^2 \bar{\mathbf{r}} \left[\frac{1}{24} \left(\frac{\partial^2 \phi^0}{\partial \bar{z}^2} \right)^2 - \frac{1}{24} \left(\frac{\partial \phi^0}{\partial \bar{z}} + h\bar{y} \right)^4 \right], \quad (\text{B4})$$

where integration is performed over the unit cell and $\phi^0(\bar{\mathbf{r}})$ is the vortex-lattice phase within London approximation. To estimate the dominating contribution, we use the circular-cell approximation for the lattice phase. In this approximation supercurrents flow radially within the cell $\bar{r} < a_c = \sqrt{2/h}$ and vanish at its boundary, so that the gauge-invariant phase gradient is given by

$$\frac{1}{\bar{r}} \frac{\partial \phi_{\text{cc}}}{\partial \alpha} = -\frac{1}{\bar{r}} + \frac{\bar{r}}{a_c^2} \quad \text{for } 0 < r < a_c$$

where $\alpha = \tan^{-1}(\bar{z}/\bar{y})$ is the polar angle meaning that $\partial \phi^0 / \partial \bar{z} + h\bar{y} \rightarrow -\cos(\alpha)(1/r - r/a_c^2)$. The integral is formally diverging at small distances. This divergency, however, is due to the vortex-core energy. To find the nontrivial correction to the lattice energy we subtract the diverging single-vortex term. The dominating contribution to the rest part is coming from the second [nonlinear] term

$$\delta u \approx -\frac{1}{24\pi} \int_0^{2\pi} d\alpha \int_0^{a_c} \bar{r} d\bar{r} \cos^4(\alpha) \left[\left(\frac{1}{\bar{r}} - \frac{\bar{r}}{a_c^2} \right)^4 - \frac{1}{\bar{r}^4} \right], \quad (\text{B5})$$

and calculation gives the following result

$$\delta u = \frac{h}{32} \ln \frac{C_h}{h}. \quad (\text{B6})$$

From fit of the numerically computed energy to this formula we obtain numerical constant $C_h \approx 110$. Note that this correction does not depend on lattice orientation with respect to the layers. Interaction with the layers also eliminates the ‘‘elliptic’’ rotation degeneracy of the lattice described in Section IV. The expansion (B5), however, is not sufficient to find the orientation-dependent correction to the energy. To obtain such correction one has to obtain the next-order expansion with respect to the gradients (6-th order terms).

Appendix C: Calculation of the orientation-dependent fluctuation correction to the free energy

In this appendix we present calculation of the entropy correction to free energy (98) based on the planar elastic

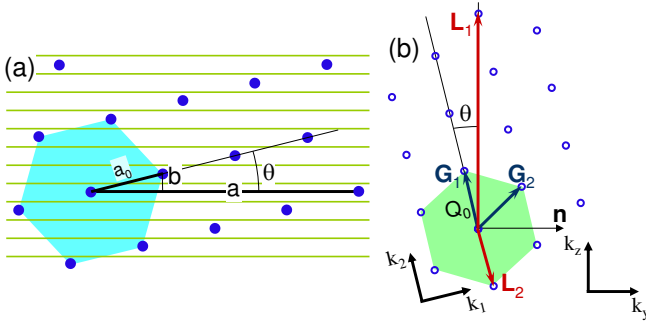


FIG. 18. *Left part:* Josephson vortex lattice in reduced coordinates rotated at finite angle θ with respect to the layers in real space so that the layers align with the crystallographic direction (3,1). *Right part:* The corresponding reciprocal lattice and illustration of two selections for the basis used in the calculation of the entropy correction: the basic wave vectors aligned with the lattice, $\mathbf{G}_{1,2}$, and the basic wave vectors aligned with the layers, $\mathbf{L}_{1,2}$.

energy (96). To facilitate calculations we again introduce the reduced wave vectors, $\tilde{\mathbf{k}}$, defined in Eq. (90) and the corresponding reciprocal-lattice vectors $\tilde{\mathbf{Q}} = (\tilde{Q}_y, \tilde{Q}_z)$. In this presentation the reciprocal lattice becomes a regular triangular lattice with the unit vector $Q_0 = \sqrt{2\pi/\sqrt{3}}$ and area of the Bravais cell equals to π . Using new variables, we represent $\Phi_{\text{JVL}}(\mathbf{k})$ in the compact reduced form as

$$\Phi_{\text{JVL}}(\mathbf{k}) = \frac{B_x^2}{4\pi\lambda_c^2} \phi_{\text{JVL}}(\tilde{\mathbf{k}}) \quad (\text{C1})$$

$$\phi_{\text{JVL}}(\tilde{\mathbf{k}}) = \sum_{\tilde{\mathbf{Q}}} \left[\frac{(\tilde{k}_y - \tilde{Q}_y)^2 + \tilde{k}_x^2}{b_x^{-1} + (\tilde{\mathbf{k}}_{yz} - \tilde{\mathbf{Q}})^2 + \tilde{k}_x^2} - \frac{\tilde{Q}_y^2}{b_x^{-1} + \tilde{Q}^2} \right] \quad (\text{C2})$$

$$\phi_{\text{JVL}}(\tilde{\mathbf{k}}) = \sqrt{\pi r} \sum_{m=-\infty}^{\infty} \left(\frac{(\tilde{k}_y - m\sqrt{\pi r})^2 + \tilde{k}_x^2}{\kappa(\tilde{k}_y - m\sqrt{\pi r}, \tilde{k}_x)} \frac{\sinh \left[2\sqrt{\pi r} \kappa(\tilde{k}_y - m\sqrt{\pi r}, \tilde{k}_x) \right]}{\cosh \left[2\sqrt{\pi r} \kappa(\tilde{k}_y - m\sqrt{\pi r}, \tilde{k}_x) \right] - \cos \left[2\pi \left(qm + \tilde{k}_z \sqrt{\frac{r}{\pi}} \right) \right]} \right. \\ \left. - \frac{\pi r m^2}{\kappa(m\sqrt{\pi r}, 0)} \frac{\sinh \left[2\sqrt{\pi r} \kappa(m\sqrt{\pi r}, 0) \right]}{\cosh \left[2\sqrt{\pi r} \kappa(m\sqrt{\pi r}, 0) \right] - \cos(2\pi qm)} \right)$$

with $\kappa(k_y, k_x) \equiv \sqrt{b_x^{-1} + k_y^2 + k_x^2}$. This formula contains only one summation which makes it convenient for numerical evaluations. On the other hand, the dependence on the rotation angle here is not obvious and is hidden in the dependence on the parameters r and q .

The sums over the reciprocal-lattice vectors in Eqs. (97) and (C2) formally diverge logarithmically at large \mathbf{Q} ($\tilde{\mathbf{Q}}$). Correspondingly, the sum over m in Eq. (C5)

where $b_x = 4\pi\lambda_{\text{ab}}\lambda_c B_x/\Phi_0 = 2(\lambda_{\text{ab}}/d)^2 h \gg 1$ and $\tilde{\mathbf{k}}_{yz} = (0, \tilde{k}_y, \tilde{k}_z)$.

We will assume that the lattice is rotated at a finite angle, θ , with respect to the layers selected in such a way that the layers are aligned with one of the crystallographic directions as sketched in Fig. 18. This means that the lattice, in general, has the form of a misaligned lattice sketched in Fig. 6a and it is characterized by the aspect ratio, $r = \gamma b/a$, and the shift parameter, q . For computing the sum over the reciprocal-lattice vectors, we will use two equivalent parametrizations illustrated in Fig. 18. The first parametrization uses expansion over the two basic vector of tilted lattice, $\tilde{\mathbf{Q}} = n\mathbf{G}_1 + m\mathbf{G}_2$ with $m, n = 0, \pm 1, \pm 2, \dots$. For such expansion we can simply represent the component of $\tilde{\mathbf{Q}}$ along the two main directions of the tilted lattice, $(\mathbf{k}_1, \mathbf{k}_2)$, shown in Fig. 18,

$$\tilde{Q}_1 = \frac{\sqrt{3}}{2} m Q_0, \quad \tilde{Q}_2 = \left(n + \frac{m}{2} \right) Q_0. \quad (\text{C3})$$

This gives $\tilde{Q}^2 = (n^2 + nm + m^2) Q_0^2$. The (y, z) -components of the wave vectors are related to the (1, 2)-components by axis rotation. For example, for the component, \tilde{k}_y , in Eq. (C2) we have $\tilde{k}_y = \cos\theta \tilde{k}_1 + \sin\theta \tilde{k}_2$. This parametrization allows us to trace naturally the dependence on the rotation angle θ . The second parametrization utilizes the basic wave vectors aligned with the layers,

$$\tilde{\mathbf{Q}} = n\mathbf{L}_1 + m\mathbf{L}_2, \quad (\text{C4}) \\ \mathbf{L}_1 = \left(0, \sqrt{\frac{\pi}{r}} \right); \quad \mathbf{L}_2 = \left(\sqrt{\pi r}, -q\sqrt{\frac{\pi}{r}} \right).$$

This basis allows us to trace easily the dependence on the lattice-structure parameters r and q . It also allows us to reduce $\phi_{\text{JVL}}(\tilde{\mathbf{k}})$ to a simpler form. Substituting presentation (C4) into Eq. (C2) and taking sum over n , we obtain

also logarithmically diverges. This divergency is due to the single-vortex tilt energy and it has to be cut at the core size, $Q_y \sim 1/\gamma d$. This energy has been considered in details in Sec. III A. We will split the reduced elastic matrix, $\phi_{\text{JVL}}(\tilde{\mathbf{k}})$, into the single-vortex, $\phi_{\text{sv}}(\tilde{k}_x)$, and interaction, $\phi_i(\tilde{\mathbf{k}})$, terms,

$$\phi_{\text{JVL}}(\tilde{\mathbf{k}}) = \phi_{\text{sv}}(\tilde{k}_x) + \phi_i(\tilde{\mathbf{k}}).$$

The single-vortex term $\phi_{\text{sv}}(\tilde{k}_x)$ can be obtained from Eq. (C2) by replacing summation over $\tilde{\mathbf{Q}}$ with integration

$$\phi_{\text{sv}}(\tilde{k}_x) = \int \frac{d^2\tilde{\mathbf{Q}}}{\pi} \left[\frac{\tilde{Q}_y^2 + \tilde{k}_x^2}{b_x^{-1} + \tilde{\mathbf{Q}}^2 + \tilde{k}_x^2} - \frac{\tilde{Q}_y^2}{b_x^{-1} + \tilde{\mathbf{Q}}^2} \right]$$

Using Eq. (31), we obtain the line-tension term in real units, $\Phi_{\text{sv}}(k_x) = \pi(B_x/\Phi_0)\varepsilon_J k_x^2 \ln(C_t/\gamma dk_x)$ with $\varepsilon_J \equiv E_0/\gamma d$ and $C_t \approx 2.86$. This corresponds to the following result for the reduced line-tension term, $\phi_{\text{sv}}(\tilde{k}_x) =$

$$(4\pi\lambda_c^2/B_x^2)\Phi_{\text{sv}}(k_x),$$

$$\phi_{\text{sv}}(\tilde{k}_x) \approx \frac{\tilde{k}_x^2}{2} \ln \frac{4.09}{h\tilde{k}_x^2}. \quad (\text{C5})$$

for $\tilde{k}_x^2 \ll 4/h$. In the interaction term, $\phi_i(\tilde{\mathbf{k}}) = \phi_{\text{JVL}}(\tilde{\mathbf{k}}) - \phi_{\text{sv}}(\tilde{k}_x)$, the logarithmic divergency is compensated and the sum over $\tilde{\mathbf{Q}}$ converges roughly at $\tilde{Q} \sim 1$. In particular, using presentation given by Eq. (C5), the interaction term can be represented as a converging sum,

$$\begin{aligned} \phi_i(\mathbf{k}) = & \sqrt{\pi r} \sum_{m=-\infty}^{\infty} \left(\frac{(\tilde{k}_y - m\sqrt{\pi r})^2 + \tilde{k}_x^2}{\kappa(\tilde{k}_y - m\sqrt{\pi r}, \tilde{k}_x)} \frac{\sinh \left[2\sqrt{\pi r} \kappa(\tilde{k}_y - m\sqrt{\pi r}, \tilde{k}_x) \right]}{\cosh \left[2\sqrt{\pi r} \kappa(\tilde{k}_y - m\sqrt{\pi r}, \tilde{k}_x) \right] - \cos \left[2\pi \left(qm + \tilde{k}_z \sqrt{\frac{r}{\pi}} \right) \right]} \right) \\ & - \sum_{\delta=\pm 1} \delta U \left[\tilde{k}_x, (m+\delta/2)\sqrt{\pi r} - \tilde{k}_y \right] \\ & - \frac{\pi r m^2}{\kappa(m\sqrt{\pi r}, 0)} \frac{\sinh \left[2\sqrt{\pi r} \kappa(m\sqrt{\pi r}, 0) \right]}{\cosh \left[2\sqrt{\pi r} \kappa(m\sqrt{\pi r}, 0) \right] - \cos(2\pi qm)} + \sum_{\delta=\pm 1} \delta U \left[0, (m+\delta/2)\sqrt{\pi r} \right] \end{aligned}$$

with

$$U[k_x, k_y] \equiv \frac{1}{2} \left[k_y \sqrt{b_x^{-1} + k_x^2 + k_y^2} + (-b_x^{-1} + k_x^2) \ln \left(k_y + \sqrt{b_x^{-1} + k_x^2 + k_y^2} \right) \right]$$

Here the terms with $U[\dots]$ originate from the single-vortex contribution $\phi_{\text{sv}}(\tilde{k}_x)$ which is properly decomposed to compensate the summation divergency. In spite of its scary look, this formula is the most suitable one for numerical calculations.

From Eq. (98) we obtain the entropy correction to the free energy in reduced form

$$\delta f_T = -\frac{T}{2\sqrt{\gamma}} \left(\frac{4\pi B_x}{\Phi_0} \right)^{3/2} \int_{-\infty}^{\infty} \frac{d\tilde{k}_x}{2\pi} \int_{\text{BZ}} \frac{d\tilde{k}_y d\tilde{k}_z}{(2\pi)^2} \ln \frac{\tilde{C}}{\phi_{\text{JVL}}(\tilde{\mathbf{k}})} \quad (\text{C6})$$

where $\int_{\text{BZ}} \dots$ notates the integral over the Brillouin zone and \tilde{C} is dimensionless constant. Integral over k_x is formally diverging. This divergency is due to short wavelength excitations in the vortex cores and it does not contribute to the angular-dependent correction. To separate the regular anisotropic correction, we subtract from the total free energy the isotropic single-vortex contribution and represent the resulting anisotropic correction as

$$\delta f_{T,a}(\theta) = -\frac{T}{\sqrt{\pi\gamma}} \left(\frac{B_x}{\Phi_0} \right)^{3/2} g_a \quad (\text{C7})$$

with

$$g_a = \int_{\text{BZ}} \frac{d^2\tilde{\mathbf{k}}_{yz}}{\pi} \int_0^\infty dk_x \ln \frac{\phi_{\text{sv}}(\tilde{k}_x)}{\phi_{\text{sv}}(\tilde{k}_x) + \phi_i(\tilde{\mathbf{k}})}. \quad (\text{C8})$$

This presentation is used in Eq. (99).

The large logarithmic factor in $\phi_{\text{sv}}(\tilde{k}_x)$ in Eq. (C5) allows us to obtain a useful approximate formula for g_a . As $\phi_i(\tilde{\mathbf{k}}) \sim 1$, integral over k_x converges at $\tilde{k}_x \sim 1/\sqrt{\ln(1/h)} \ll 1$ meaning that for a log-accuracy estimate we can neglect \tilde{k}_x -dependence of $\phi_i(\tilde{\mathbf{k}})$. Evaluating the integral over k_x , we obtain

$$g_a \approx -\frac{\sqrt{2}}{\sqrt{\ln(A/h)}} \int_{\text{BZ}} d^2\tilde{\mathbf{k}}_{yz} \sqrt{\phi_i(\tilde{\mathbf{k}}_{yz})}. \quad (\text{C9})$$

with $A \sim 1$. If we neglect small parameter b_x^{-1} in $\phi_i(\tilde{\mathbf{k}}_{yz})$ then the integral in this formula becomes field independent and the only field dependence of g_a for $h \rightarrow 0$ is given by the factor $[\ln(A/h)]^{-1/2}$.

We numerically computed the reduced entropy correction g_a for different lattice orientations and reduced fields h . Example of the angular dependence of g_a for $h = 0.0067$ is shown in the inset of figure 19. We found that in the range $0.001 < h < 0.1$ the orientation-dependent part of g_a can be well fitted by the formula (100). The dependence $g_6(h)$ is plotted in figure 19. Positive sign of $g_6(h)$ means that the fluctuations give the largest negative contribution for $\theta = 0$, i.e., they indeed favor the aligned lattice (1,0). We also can see that the effect occurs to be quantitatively rather small, at least in the considered Gaussian-fluctuations regime.

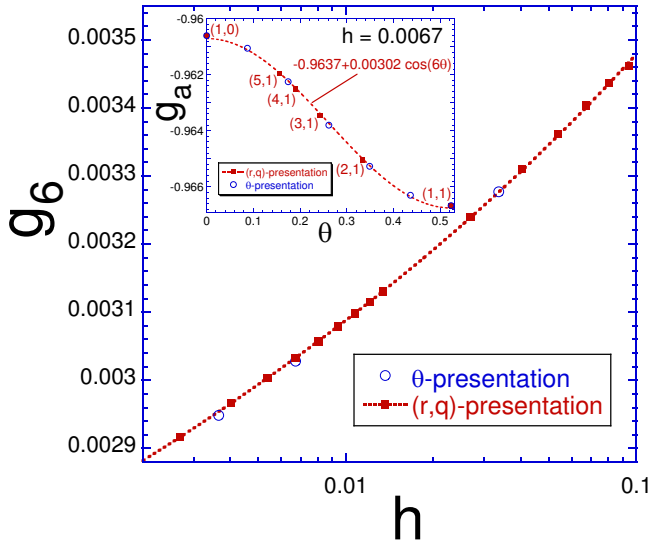


FIG. 19. Inset shows the example of the numerically computed angular dependence of the reduced entropy connection $g_a(\theta)$ defined by Eq. (C8) for $h = 0.0067$. Solid squares show results obtained using representation for fixed lattice parameters r and q given by Eq. (C6). This computation is done for layers oriented along the crystal directions (m, n) which are also shown in the plot. Open symbols are obtained using representation with the explicit dependence on the lattice rotation angle θ using the expansion (C3). Dashed line is the fit to the formula $g_0 + g_6 \cos(6\theta)$. The main plot shows the field dependence of the coefficient g_6 and the corresponding fit in Eq. (100).

-
- ¹ B. D. Josephson, Phys. Letters **1**, 251 (1962).
² J. G. Bednorz and K. A. Muller, Z. Phys. B **64**, 189 (1986).
³ M. K. Wu, J. R. Ashburn, C. J. Torng, P. H. Hor, R. L. Meng, L. Gao, Z. J. Huang, Y. Q. Wang, and C. W. Chu, Phys. Rev. Lett. **58**, 908 (1987).
⁴ H. Maeda, Y. Tanaka, M. Fukutomi, and T. Asano, Japan. J. Appl. Phys. **27**, L209 (1988).
⁵ C. W. Chu, J. Bechtold, L. Gao, P. H. Hor, Z. J. Huang, R. L. Meng, Y. Y. Sun, Y. Q. Wang, and Y. Y. Xue, Phys. Rev. Lett. **60**, 941 (1988).
⁶ J. Wilson and A. Yoffe, Adv. in Phys. **18**, 193 (1969).
⁷ L. N. Bulaevskii, Usp. Fiz. Nauk **116**, 449 (1975), [*Sov. Phys.-Usp.* **18**, 514 (1976)].
⁸ T. Ishiguro and K. Yamaji, *Organic Superconductors* (Springer, Berlin, 1990) chapter 5.
⁹ J. Singleton, Rep. Prog. Phys. **63**, 1111 (2000).
¹⁰ Y. Kamihara, T. Watanabe, M. Hirano, and H. Hosono, J. Am. Chem. Soc. **130**, 3296 (2008).
¹¹ D. C. Johnston, Adv. in Phys. **59**, 803 (2010).
¹² P. C. Canfield and S. L. Bud'ko, Ann. Rev. of Cond. Mat. Phys. **1**, 27 (2010).
¹³ G. R. Stewart, Rev. Mod. Phys. **83**, 1589 (2011).
¹⁴ X. H. Chen, T. Wu, G. Wu, R. H. Liu, H. Chen, and D. F. Fang, Nature **453**, 761 (2008).
¹⁵ P. J. W. Moll, L. Balicas, V. Geshkenbein, G. Blatter, J. Karpinski, N. D. Zhigadlo, and B. Batlogg, Nature Materials **12**, 134 (2013).
¹⁶ X. Zhu, F. Han, G. Mu, P. Cheng, B. Shen, B. Zeng, and H.-H. Wen, Phys. Rev. B **79**, 220512 (2009).
¹⁷ H. Ogino, Y. Matsumura, Y. Katsura, K. Ushiyama, S. Horii, K. Kishio, and J. ichi Shimoyama, Supercond. Sci. Technol. **22**, 075008 (2009).
¹⁸ S. Sato, H. Ogino, N. Kawaguchi, Y. Katsura, K. Kishio, J. ichi Shimoyama, H. Kotegawa, and H. Tou, Supercond. Sci. Technol. **23**, 045001 (2010).
¹⁹ G. Blatter, M. V. Feigelman, V. B. Geshkenbein, A. I. Larkin, and V. M. Vinokur, Rev. Mod. Phys. **66**, 1125 (1994).
²⁰ D. Feinberg, J. Physique III **4**, 169 (1994).
²¹ E. H. Brandt, Rep. Prog. Phys. **58**, 1465 (1995).
²² T. Nattermann and S. Scheidl, Adv. Phys. **49**, 607 (2000).
²³ G. Blatter and V. B. Geshkenbein, in *The Physics of Superconductors*, Vol 1: Conventional and High- T_c Superconductors, edited by K. Bennemann and J. Ketterson (Springer, Berlin, 2003) p. 726, ed Bennemann K H and Ketterson J B.
²⁴ L. J. Campbell, M. M. Doria, and V. G. Kogan, Phys. Rev. B **38**, 2439 (1988).

- ²⁵ L. Bulaevskii and J. R. Clem, Phys. Rev. B **44**, 10234 (1991).
- ²⁶ In the literature the layer plane and the axis perpendicular to the layers are frequently called “ab plane” and “c axis”.
- ²⁷ J. R. Clem, Journal of Superconductivity **17**, 613 (2004).
- ²⁸ G. J. Dolan, F. Holtzberg, C. Feild, and T. R. Dinger, Phys. Rev. Lett. **62**, 2184 (1989).
- ²⁹ M. Oussena, P. A. J. de Groot, R. Gagnon, and L. Taillefer, Phys. Rev. Lett. **72**, 3606 (1994).
- ³⁰ A. A. Zhukov, H. Küpfer, G. K. Perkins, A. D. Caplin, T. Wolf, K. I. Kugel, A. L. Rakhmanov, M. G. Mikheev, V. I. Voronkova, M. Kläser, and H. Wühl, Phys. Rev. B **59**, 11213 (1999).
- ³¹ S. N. Gordeev, A. A. Zhukov, P. A. J. de Groot, A. G. M. Jansen, R. Gagnon, and L. Taillefer, Phys. Rev. Lett. **85**, 4594 (2000).
- ³² C. A. Bolle, P. L. Gammel, D. G. Grier, C. A. Murray, D. J. Bishop, D. B. Mitzi, and A. Kapitulnik, Phys. Rev. Lett. **66**, 112 (1991).
- ³³ M. Tokunaga, T. Tamegai, Y. Fasano, and F. de la Cruz, Phys. Rev. B **67**, 134501 (2003).
- ³⁴ A. Grigorenko, S. Bending, T. Tamegai, S. Ooi, and M. Henini, Nature **414**, 728 (2001).
- ³⁵ T. Matsuda, O. Kamimura, H. Kasai, K. Harada, T. Yoshida, T. Akashi, A. Tonomura, Y. Nakayama, J. Shimoyama, K. Kishio, T. Hanaguri, and K. Kitazawa, Science **294**, 2136 (2001).
- ³⁶ A. Tonomura, H. Kasai, O. Kamimura, T. Matsuda, K. Harada, T. Yoshida, T. Akashi, J. Shimoyama, K. Kishio, T. Hanaguri, K. Kitazawa, T. Masui, S. Tajima, N. Koshizuka, P. L. Gammel, D. Bishop, M. Sasase, and S. Okayasu, Phys. Rev. Lett. **88**, 237001 (2002).
- ³⁷ V. K. Vlasko-Vlasov, A. Koshelev, U. Welp, G. W. Crabtree, and K. Kadowaki, Phys. Rev. B **66**, 014523 (2002); in “*Proc. NATO Advanced Research Workshop on Magneto-Optical Imaging (Oystese, Norway, Aug. 2003)*” vol. 142 (Kluwer Academic, Dordrecht, 2002) p. 39, ed Johansen T H and Shantsev D V.
- ³⁸ M. Tokunaga, M. Kobayashi, Y. Tokunaga, and T. Tamegai, Phys. Rev. B **66**, 060507 (2002).
- ³⁹ S. J. Bending and M. J. W. Dodgson, J. Phys.: Condens. Matt. **17**, R955 (2005).
- ⁴⁰ J. U. Lee, J. E. Nordman, and G. Hohenwarter, Appl. Phys. Lett. **67**, 1471 (1995); J. U. Lee, P. Gup-tasarma, D. Hornbaker, A. El-Kortas, D. Hinks, and K. E. Gray, Appl. Phys. Lett. **71**, 1412 (1997).
- ⁴¹ G. Hechtfisher, R. Kleiner, A. V. Ustinov, and P. Müller, Phys. Rev. Lett. **79**, 1365 (1997); G. Hechtfisher, R. Kleiner, K. Schlenga, W. Walkenhorst, P. Müller, and H. L. Johnson, Phys. Rev. B **55**, 14638 (1997).
- ⁴² Y. I. Latyshev, M. B. Gaifullin, T. Yamashita, M. Machida, and Y. Matsuda, Phys. Rev. Lett. **87**, 247007 (2001).
- ⁴³ Y. I. Latyshev, A. E. Koshelev, and L. N. Bulaevskii, Phys. Rev. B **68**, 134504 (2003).
- ⁴⁴ S. M. Kim, H. B. Wang, T. Hatano, S. Urayama, S. Kawakami, M. Nagao, Y. Takano, T. Yamashita, and K. Lee, Phys. Rev. B **72**, 140504 (2005).
- ⁴⁵ S. Ooi, T. Mochiku, and K. Hirata, Phys. Rev. Lett. **89**, 247002 (2002).
- ⁴⁶ B. Y. Zhu, H. B. Wang, S. M. Kim, S. Urayama, T. Hatano, and X. Hu, Phys. Rev. B **72**, 174514 (2005).
- ⁴⁷ Y. Latyshev, V. Pavlenko, A. P. Orlov, and X. Hu, Pis'ma v ZhETF **82**, 251 (2005), [*JETP Lett.* **82**, 232 (2005)].
- ⁴⁸ S. O. Katterwe and V. M. Krasnov, Phys. Rev. B **80**, 020502 (2009).
- ⁴⁹ I. Kakeya, Y. Kubo, M. Kohri, M. Iwase, T. Yamamoto, and K. Kadowaki, Phys. Rev. B **79**, 212503 (2009).
- ⁵⁰ Here e is chosen to be positive, $e > 0$, i.e., the charge of an electron is $-e$.
- ⁵¹ W. E. Lawrence and S. Doniach, in *Proc. 12th Int. Conf. Low Temp. Phys., Kyoto, Japan*, edited by E. Kanda (1970) p. 361.
- ⁵² L. N. Bulaevskii, Zh. Eksp. Teor. Fiz. **64**, 2241 (1973), [*Sov. Phys.-JETP* **37**, 1133 (1973)].
- ⁵³ B. D. Josephson, Adv. Phys. **14**, 419 (1965).
- ⁵⁴ This characteristic length was noted soon after the discovery of the Josephson effect⁸⁶.
- ⁵⁵ J. R. Clem and M. Coffey, Phys. Rev. B **42**, 6209 (1990).
- ⁵⁶ A. E. Koshelev, Phys. Rev. B **48**, 1180 (1993).
- ⁵⁷ J. R. Clem, M. W. Coffey, and Z. Hao, Phys. Rev. B **44**, 2732 (1991).
- ⁵⁸ R. A. Klemm and J. R. Clem, Phys. Rev. B **21**, 1868 (1980).
- ⁵⁹ G. Blatter, V. B. Geshkenbein, and A. I. Larkin, Phys. Rev. Lett. **68**, 875 (1992).
- ⁶⁰ B. I. Ivlev, N. B. Kopnin, and V. L. Pokrovskii, J. Low Temp. Phys. **80**, 187 (1990).
- ⁶¹ L. S. Levitov, Phys. Rev. Lett. **66**, 224 (1992).
- ⁶² M. F. Laguna, D. Dominguez, and C. A. Balseiro, Phys. Rev. B **62**, 6692 (2000).
- ⁶³ B. M. Stewart, *Theory of numbers* (The Macmillan Company, New York, 1964).
- ⁶⁴ M. Ichioka, Phys. Rev. B **51**, 9423 (1995).
- ⁶⁵ A. E. Koshelev, Proceedings of FIMS/ITS-NS/CTC/PLASMA 2004, Tsukuba, Japan, Nov. 2428, 2004; arXiv:cond-mat/0602341.
- ⁶⁶ Y. Ionomura and X. Hu, Phys. Rev. B **74**, 024504 (2006).
- ⁶⁷ R. Ikeda and K. Isotani, Journ. Phys. Soc. Japan **68**, 599 (1999).
- ⁶⁸ S. E. Korshunov, Europhys. Lett. **15**, 771 (1990).
- ⁶⁹ S. E. Korshunov and A. I. Larkin, Phys. Rev. B **46**, 6395 (1992).
- ⁷⁰ A. E. Koshelev, Phys. Rev. B **66**, 224514 (2002); Phys. Rev. B **75**, 214513 (2007).
- ⁷¹ M. Machida, Phys. Rev. Lett. **90**, 037001 (2003); Phys. Rev. Lett. **96**, 097002 (2006).
- ⁷² A. Irie and G. Oya, Supercond. Sci. Technol. **20**, S18 (2007).
- ⁷³ K. B. Efetov, Zh. Eksp. Teor. Fiz. **76**, 1781 (1979), [*Sov. Phys.-JETP* **49**, 905 (1979)].
- ⁷⁴ B. Horovitz, Phys. Rev. B **47**, 5964 (1993).
- ⁷⁵ L. Balents and D. R. Nelson, Phys. Rev. B **52**, 12951 (1995).
- ⁷⁶ L. Balents and L. Radzihovsky, Phys. Rev. Lett. **76**, 3416 (1996).
- ⁷⁷ X. Hu, M. Luo, and Y. Ma, Phys. Rev. B **72**, 174503 (2005).
- ⁷⁸ X. Hu and M. Tachiki, Phys. Rev. Lett. **85**, 2577 (2000).
- ⁷⁹ X. Hu and M. Tachiki, Phys. Rev. B **70**, 064506 (2004).
- ⁸⁰ As in most theoretical papers, the temperature is measured in energy units.
- ⁸¹ A. E. Koshelev, Phys. Rev. B **50**, 506 (1994).
- ⁸² W. K. Kwok, J. Fendrich, U. Welp, S. Fleshler, J. Downey, and G. W. Crabtree, Phys. Rev. Lett. **72**, 1088 (1994).
- ⁸³ J. Villain, R. Bidaux, J. Carton, and R. Conte, J. Phys. (France) **41**, 1263 (1980).
- ⁸⁴ V. L. Pokrovskii and G. V. Uimin, Zh. Eksp. Teor. Fiz. **65**, 1961 (1973), [*Sov. Phys.-JETP* **38**, 847 (1974)].
- ⁸⁵ L. I. Glazman and A. E. Koshelev, Zh. Eksp. Teor. Fiz **97**,

1371 (1990), [*Sov. Phys.-JETP* **70**, 774 (1990)].

⁸⁶ R. A. Ferrell and R. E. Prange, *Phys. Rev. Lett.* **10**, 479 (1963).